Received 29 January 2024, accepted 14 February 2024, date of publication 20 February 2024, date of current version 27 February 2024.

Digital Object Identifier 10.1109/ACCESS.2024.3367753

RESEARCH ARTICLE

Enhancing Individual UAV Path Planning With Parallel Multi-Swarm Treatment Coronavirus Herd Immunity Optimizer (PMST-CHIO) Algorithm

ALLOUANI FOUAD[1], ABDELAZIZ ABBOUDI[2], CHRIS HUYCK[3], XIAO-ZHI GAO[4], SOFIANE BOUOUDEN[1], ILYES BOULKAIBET[5], NADHIRA KHEZAMI[5], AND HANEN SHALL[5]

[1]Laboratory of SATIT, Department of Industrial Engineering, University of Khenchela Abbes Laghrour, Khenchela 40004, Algeria
[2]Department of Mechanical Engineering, University of Khenchela Abbes Laghrour, Khenchela 40004, Algeria
[3]School of Science and Technology, Middlesex University, NW4 4BT London, U.K.
[4]School of Computing, University of Eastern Finland, 70211 Kuopio, Finland
[5]College of Engineering and Technology, American University of the Middle East, Egaila 54200, Kuwait

Corresponding author: Allouani Fouad (Allouani_fouad@univ-khenchela.dz)

ABSTRACT This paper introduces the PMST-CHIO, a novel variant of the Coronavirus Herd Immunity Optimizer (CHIO) algorithm, exclusively tailored for individual unmanned aerial vehicle (UAV) path planning in complex 3D environments. While acknowledging and building upon the foundational principles derived from UAV swarm path planning research, the PMST-CHIO distinctively focuses on optimizing the trajectory of single UAVs. It innovatively integrates a parallel multi-swarm treatment mechanism, enhancing the standard CHIO's exploration and exploitation capabilities significantly. This mechanism diverges from the swarm-based approaches by deploying multiple instances of the CHIO optimizer, each functioning autonomously within its sub-swarm, thereby facilitating independent path planning for individual UAVs. These multiple CHIO instances or CHIO candidates, operate in concert to determine the optimal and collision-free routes, taking into account the unique characteristics of individual UAVs and the intricacies of the service area. The algorithm incorporates two key mechanisms: 1) global exploitation, employing the best solution identified by the highest performing CHIO candidate across the swarms; and 2) strategic shift from parallel multi-swarm exploration to focused exploration by the top-performing CHIO candidate after a specific iteration threshold is reached. This adaptation significantly improves the algorithm's global search efficiency, convergence behavior, and navigational accuracy under challenging environments. Extensive simulations and comparative studies validate that the PMST-CHIO can effectively overcome the limitations of the standard CHIO algorithm, yielding safer, shorter, and more compliant flight paths for individual UAVs in intricate 3D landscapes.

INDEX TERMS Coronavirus Herd Immunity Optimizer (CHIO), flight path optimization and safety, unmanned aerial vehicles (UAVs) path planning.

I. INTRODUCTION

Unmanned Aerial Vehicles (UAVs) are autonomous flight systems that can operate under remote control or via integrated onboard computers. These vehicles provide a cost-effective, adaptable, and safer alternative to manned aircraft, which are particularly useful in hazardous or inaccessible areas. UAVs have gained extensive application in both civilian and military sectors due to these advantages. In civilian applications, they are instrumental in tasks like agricultural

The associate editor coordinating the review of this manuscript and approving it for publication was Yang Tang.

TABLE 1. List of acronyms and their meanings.

Acronym	Meaning
ABC	Artificial Bee Colony
ACVO	The Anti-Coronavirus Optimization algorithm
ALO	Ant Lion Optimizer
BA	Bat algorithm
BBO	Biogeography-Based Optimization
BS	Base Station
C-19BOA	The COVID-19 Based Optimization Algorithm
CESMO	Cooperative Co-Evolution-based Spider Monkey Optimization algorithm
CHIO	The Coronavirus Herd Immunity Optimizer
CMOA	The Coronavirus Metamorphosis Optimization Algorithm
CMPA	The Coronavirus Mask Protection Algorithm
COVID-19	Coronavirus Disease 2019
COVIDOA	The Coronavirus Optimization Algorithm
CS	Cuckoo Search
CVO	The Corona Virus Optimization
CVOA	Coronavirus Optimization Algorithm
DA	Dragonfly Algorithm
DE	Differential Evolution
DLC + RPSO	Double-Layer Coding model and Rotating Particle Swarm Optimization
FWA	Firework Algorithm
GA	Genetic Algorithm
GSO	Glowworm Swarm Optimization
GWO	Grey Wolf Optimizer
HR-MAGA	Hierarchical Recursive-Multi Agent Genetic Algorithm
HS	Harmony Search
HSGWO-MSOS	Combination between Simplified GWO and Modified SOS
MFO	Moth Flame Optimization
MVO	Multi-Verse Optimizer algorithm
NEH	The Nawaz-Enscore-Ham method
NSGA-II	Non-dominated Sorting Genetic Algorithm II
PMST-CHIO	Parallel Multi-Swarm Treatment Coronavirus Herd Immunity Optimizer
PSOGA	Particle Swarm Optimization – Genetic Algorithm
QoS	Quality of Service
RSUs	Multiple Roadside Units
SA	Simulated Annealing
SIC+	(SIC following QoS): This is another path planning strategy that first optimizes search and inform tasks together and then finds the optimum positions for monitoring
SICQ	(SIC with QoS): This refers to a path planning strategy that optimizes search, inform, and monitor tasks simultaneously
SLR	The Straight-Line Rate
SOS	Symbiotic Organisms Search
SPSO	Spherical Vector-based PSO
UAVs	Unmanned Aerial Vehicles
UCAV	Unmanned Combat Aerial Vehicle
WHO	The World Health Organization
WOA	Whale Optimization Algorithm

monitoring, aerial photography, surveillance, expedited transport, and forest fire detection and containment. In the military domain, UAVs are pivotal for high-risk missions like reconnaissance and intelligence gathering, serving as alternatives to manned flights. A critical aspect distinct to individual UAV operations, as opposed to UAV swarms, is the necessity of efficient and precise path planning. This process entails developing a collision-free trajectory between two points, considering flight conditions and constraints. Path planning for individual UAVs differs significantly from swarm path planning. While swarm path planning involves coordinating multiple UAVs to achieve a collective goal, individual UAV path planning focuses on optimizing a single vehicle's trajectory. This distinction is crucial in our research as we concentrate on optimizing path planning for individual UAVs. We acknowledge the insights gained from UAV swarm research but adapt and refine these strategies for singular UAV applications. Our approach treats path planning as a multi-constraint optimization problem, aiming to minimize flight costs and comply with operational constraints, thereby ensuring efficient and safe UAV missions.

Meta-heuristic algorithms offer an advanced solution to complex combinatorial optimization problems, often surpassing the performance of traditional methods. These algorithms excel at thoroughly exploring search spaces, often unearthing optimal or nearly optimal solutions. Their efficacy is particularly noticeable in the realm of UAV path planning. Meta-heuristic algorithms broadly fall into two categories:

TABLE 2. Parameters definition.

Section	Parameter	Signification
Section II	$F_1(X_i)$	The cost function for the path length
	$P_{i,j}$, $P_{i,j+1}$	Two adjacent path points
	K	A set of all threats
	C_k	Centre coordinate of an obstacle
	R_k	Radius of an obstacle
	D	The size of the UAV
	d_k	Distance between the UAV and the center of each threat
	$F_2(X_i)$	The threat cost
	S	Crash area
	$F_3(X_i)$	The altitude cost
	h_{ij}	Flying height of the device relative to the ground
	h_{min}	The minimum height
	h_{max}	The maximum height
	ϕ_{ij}	The turning angle
	ψ_{ij}	The climbing angle
	$F_4(X_i)$	The smoothing cost
Section III	C_0	The number of initial infection cases triggered by an individual
	HIS	The population size
	Max_{Itr}	The total number of iterations
	n	The problem dimensionality
	BRr	The basic reproduction rate
	Max_{Age}	The maximum age of infected cases
	HIP	The herd immunity population
	S_v	The status vector
Section IV	N_{Sub_HIP}	Number of herd immunity sub-populations
	Max_{P_Itr}	The threshold iteration
	Run_{max}	Maximum algorithm run times
	$n_{threats}$	Number of Threats on the Battlefield
	Path_j^{itr}	3D Coordinates of Path Nodes during iteration (Itr) relative to candidate solution j
	$\text{Path}_{j^{best}}^{Max_{Itr}}$	3D Coordinates of Path Nodes after completing the truing stage, i.e., when $iter = Max_{Itr}$, relative to the best candidate solution j^{best}

single-based and population-based strategies. Single-based strategies, like the work of Du et al. [1], apply modified versions of existing algorithms, such as the Tabu search algorithm, to address intricate issues like multi-UAV path planning. Specifically, Du et al. integrated the Nawaz-Enscore-Ham (NEH) method into the Tabu search algorithm to tackle this problem. Population-based strategies are further divided into four unique categories: evolutionary-based, swarm intelligence-based, physics-based, and human-based algorithms. Evolutionary-based algorithms mimic the natural selection process. Swarm intelligence-based algorithms are inspired by collective behavior found in nature. Physics-based techniques model themselves after physical systems. Finally, human-based algorithms utilize human intuition and expertise.

Within the first category of population-based approaches, Yang et al. [2] introduced the Hierarchical Recursive Multiagent Genetic Algorithm (HR-MAGA) for UAV path planning in dynamic environments. HR-MAGA employs a hierarchical recursive optimization method, enhancing the search efficiency of evolutionary algorithms and adaptability to environmental changes. The algorithm outperforms its predecessors, including the Path Multiagent Genetic Algorithm (P-MAGA) and the standard Genetic Algorithm (GA), in generating efficient, collision-free paths. This advancement is particularly notable in complex and evolving environments, demonstrating superior global optimization and real-time response capabilities. In a separate study, Hayat et al. [3] proposed two methods, SICQ and SIC+, aimed at enhancing UAV path planning via simultaneous information sharing and Quality of Service (QoS) connectivity. These methods were assessed in a comparatively simpler setting, featuring one base station and various operational UAVs. The results suggested that SIC+ outpaced SICQ in coverage and information sharing time. Moreover, Chawra and Gupta [4] implemented a Differential Evolution (DE) algorithm to optimize the path planning of multiple UAVs for data collection in a cluster-based Wireless Sensor Network. The efficacy of the DE algorithm was validated in four unique areas, each containing a single Base Station (BS) and one operational UAV. The findings confirmed that the DE algorithm was superior to both GA and NSGA-II in optimizing path length and minimizing travel time. In summary, population-based approaches furnish a diverse range of algorithms to optimize UAV path planning for various applications, each with its unique strengths and weaknesses. Regardless, experimental outcomes have consistently shown the high performance of these algorithms, highlighting their efficiency in path generation, travel time reduction, and the enhancement of coverage and information sharing time.

Recent research has focused on harnessing swarm intelligence-based algorithms to solve the complex problem of UAV path planning, particularly in challenging and hazardous regions. For instance, Liu et al. [5] introduced a novel three-dimensional path planning algorithm for the unmanned aerial vehicles (UAVs), which combines adaptive sensitivity decision operators with particle swarm optimization (PSO). The algorithm addresses the issues of local optima and slow convergence by constructing an adaptive sensitivity decision area and limiting the search space of particles. It also improves the searching accuracy by considering relative particle directivity. The algorithm's objective function accounts for the distance to the destination and UAV self-constraints. Experimental results show that it outperforms other tested optimization algorithms, with an average improvement of 35.4% in the path cost and 9.6% in the straight-line rate (SLR). This algorithm provides efficient and effective path planning for the UAVs.

In another study, Qu et al. [6] presented a hybrid Grey Wolf Optimization (GWO) algorithm, named HSGWO-MSOS, blending Simplified GWO and Modified SOS to address the path planning problem for UAVs in intricate and dangerous territories. Experimental findings suggested that the HSGWO-MSOS algorithm efficiently and safely charted a path, surpassing other algorithms such as GWO, SOS, and Simulated Annealing (SA). Similarly, Zhu et al. [7] put forth a Cooperative Co-Evolution-based Spider Monkey Optimization algorithm (CESMO) to handle the Unmanned Combat Aerial Vehicle (UCAV) path planning challenge, specifically for obstacle avoidance. This algorithm was evaluated against ten swarm intelligence algorithms over 36 test cases. The experimental findings highlighted the robustness and competitiveness of CESMO in solving the UCAV path planning problem. Furthermore, Jia et al. [8] devised a unique PSO variant, termed RPSO, utilizing a new strategy of rotating particles in high-dimensional space to locate targets. This algorithm was employed to resolve the UCAV path planning problem using a novel combat field model called the Double-Layer Coding model for path planning. Experimental outcomes showed that the proposed DLC + RPSO method consistently produced viable flight paths in complex scenarios. In summary, recent studies have produced numerous efficient and effective swarm intelligence-based algorithms, that are valuable in solving the intricate problem of UAV path planning in hazardous areas.

In their study, Phung and Ha [9] introduce the Spherical Vector-based Particle Swarm Optimization (SPSO) algorithm, tailored for the efficient and safe determination of UAV flight paths. This algorithm integrates a comprehensive cost function that accounts for key factors such as path length, potential threats, turn and climb/dive angles, and flight altitude, ensuring both safety and efficiency in UAV navigation. SPSO's effectiveness is thoroughly evaluated against various particle swarm optimization variants and leading metaheuristic algorithms in multiple scenarios. The findings reveal that it can consistently surpass these alternatives in the majority of the tested scenarios. Furthermore, the research work includes practical experiments, confirming the real-world feasibility of the UAV paths derived from the SPSO algorithm.

The integration of human cognitive mechanisms into the ABC algorithm, as developed by Han et al. [10], significantly enhances its autonomy and intelligence, particularly for UAV path planning. This evolutionary learning framework marks a considerable advancement in adapting the algorithm to be more responsive and adaptable. In a separate yet notable study [11], the ABC algorithm has been refined with a multi-strategy synthesis designed specifically for UAV path planning, which optimizes the UAVs' ability to navigate complex environments by rapidly identifying the most efficient routes. Chen et al. [12] introduced an innovative adaptation known as the opposition-based learning ABC algorithm, tailored for UAV path planning. It is particularly effective in optimizing the collection of building surface data based on minimal imagery, demonstrating its practicality in real-world applications. Another breakthrough in the field comes with the development of a parallel ABC algorithm, focused on unmanned combat aerial vehicles (UCAVs). The authors [13] highlight the algorithm's critical role in military operations, emphasizing its cost-effectiveness and operational efficiency. Furthermore, the research led by Yu et al. [14] showcases the simplicity and robustness of the ABC algorithm in UAV trajectory planning, particularly emphasizing its relevance in modern warfare scenarios. Their work underlines the increasing significance of UAVs and the necessity for efficient path planning solutions. Collectively, these studies underscore the ABC algorithm's versatility and effectiveness in tackling diverse challenges in UAV path planning, solidifying its status as an invaluable asset in both civilian and military realms.

Physics-based meta-heuristic algorithms have shown significant utility in addressing the path planning problem for UAVs. An example of this is the Multi-Verse Optimizer (MVO) algorithm [15], used to optimize UAV travel routes in two-dimensional space while ensuring end-to-end Quality of Service (QoS). The MVO algorithm's performance was evaluated against other gradient-free meta-heuristics, including ALO, DA, GWO, MFO, and WOA. Simulations showed that MVO outperformed these algorithms in convergence rate, fitness function value distribution, and computational efficiency. Additionally, Jain et al. [16] proposed a modified version of the MVO algorithm to tackle the UAV path planning challenge in complex environments, catering to both single and multiple UAV contexts. Experimental results indicated that this enhanced MVO algorithm outperformed Glowworm Swarm Optimization (GSO) and Biogeography-Based Optimization (BBO) in terms of path length and cost. However, it is worth noting that the computation time for the modified MVO was higher than that of BBO in the single UAV scenario, while it was similar in multiple UAV situations. The superior performance of the modified MVO algorithm is likely due to the improvements made to the original algorithm, emphasizing the value of continuous refinement in developing more effective solutions.

In the realm of human-based meta-heuristic algorithms, two prominent studies merit discussion. The first is a study conducted by Adis Alihodzic, proposing a Modified Firework Algorithm (FWA) [17] to solve the UAV path planning problem. This enhanced FWA algorithm uniquely integrates new feasibility rules. The algorithm was tested in a two-dimensional environment, featuring eight obstacles. Simulation outcomes revealed that the modified FWA algorithm outperformed several well-known algorithms such as BA, CS, DE, and PSO, achieving better path cost optimization and reduced execution time. The second study, undertaken by Binol et al. [18], focuses on the path planning problem for multiple UAVs tasked with collecting data from pre-deployed roadside units (RSUs) in various scenarios. Given the constraints of UAV battery capacity and mission time, which may not be sufficient to visit all RSUs, two problems are formulated: one to equalize travel distances among UAVs and another to minimize the total path length. The study proposes two modified metaheuristic-based solutions with unique evolutionary operators. The experimental results reveal that the proposed Harmony Search (HS) algorithm surpasses the Genetic Algorithm (GA) in terms of cost-effectiveness, especially in complex scenarios, and demonstrates quicker convergence in simpler search processes.

In the dynamic landscape of our modern era, an intriguing development has been the emergence of numerous meta-heuristic algorithms inspired by the nature and behavior of the COVID-19 pandemic. These innovative algorithms are as complex as the virus they emulate, subtly mirroring its characteristics to optimize processes and find solutions across a broad spectrum of domains. Currently, there are eight distinct meta-heuristic optimization algorithms, each of which incorporates a unique aspect of the infamous pandemic. These are not just theoretical explorations but practical innovations named as follows: the Coronavirus Optimization Algorithm (CVOA) [19], the Coronavirus Herd Immunity Optimizer (CHIO) [20], the Corona Virus Optimization (CVO) [21], the Anti-Coronavirus Optimization (ACVO) algorithm [22], the Coronavirus Optimization Algorithm (COVIDOA) [23], the COVID-19 Based Optimization Algorithm (C-19BOA) [24], the Coronavirus Metamorphosis Optimization Algorithm (CMOA) [25], and the Coronavirus Mask Protection Algorithm (CMPA) [26]. These algorithms demonstrate their notably improved performance in solving various optimization challenges. Particularly, the CHIO algorithm stands out amongst these innovations due to its dynamism and adjustable control parameters, enabling efficient investigation and exploration of diverse search spaces. Nevertheless, it is critical to approach these exciting developments with a level of caution. Given their early stages, these algorithms need comprehensive testing and validation across different scenarios. Rigorous examination will help confirm their robustness and effectiveness before being broadly applied, ensuring they remain not just inventive, but also trustworthy and efficient tools for problem-solving in our rapidly changing world.

In this paper, we present PMST-CHIO, a sophisticated adaptation of the CHIO algorithm specifically developed for path planning of individual UAVs in challenging three-dimensional spaces. The innovation of the PMST-CHIO is its parallel multi-swarm treatment mechanism. Unlike UAV swarm path planning that involves coordinating multiple UAVs, our approach focuses on enhancing the path planning capabilities of a single UAV. The mechanism operates with multiple CHIO candidates, each exploring potential solutions independently within their respective sub-swarms. This process allows every CHIO candidate, an instance of the CHIO optimizer, to investigate diverse solutions with distinct parameters, thus enriching the variety in the search process. Crucially, the PMST-CHIO enhances global exploitation and convergence by initially utilizing solutions from the most effective CHIO candidate. After reaching a predetermined iteration threshold, the focus shifts from parallel exploration across all candidates to concentrated exploration by the leading candidate, which can significantly improve the exploration and exploitation potential of the standard CHIO algorithm. Moreover, it is finely tuned to meet the specific safety and flight constraints of individual UAVs navigating complex 3D environments, a clear departure from the swarm-based path planning approaches. The paper is structured as follows: Section II discusses the threat environment model for UAV path planning. Section III focuses solely on the Coronavirus Herd Immunity Optimizer (CHIO) algorithm. The adapted PMST-CHIO algorithm is thoroughly explained in Section IV. Section V shows experimental simulations to validate the PMST-CHIO algorithm in UAV path planning. Section VI critically assesses the PMST-CHIO algorithm, its pros and cons, and future improvements, particularly for single UAV operations. Finally, Section VII concludes the paper with overall findings and implications for UAV path planning.

II. THREAT ENVIRONMENT MODEL

The threat environment model developed within this section has been obtained from the theoretical frameworks and insights delineated by Phung and Ha [9].

A. OPTIMAL PATH

The path planning operation for UAVs is treated as an optimization problem that involves choosing different criteria depending on various application conditions to achieve the optimal solution. One of the main parameters for optimizing the path is the path length. Specifically, in this study, we aim to minimize the path length and use the flight path X_i to illustrate all n path points that the flight device must follow. It should be noted that each path point corresponds to a path node on the map. The cost function for the path length is as follows:

$$F_1(X_i) = \sum_{j=1}^{n-1} \left\| \overrightarrow{P_{i,j}P_{i,j+1}} \right\| \tag{1}$$

The expression $\|\overrightarrow{P_{i,j}P_{i,j+1}}\|$ represents the Euclidean distance between two adjacent path points, namely $P_{i,j}$ and $P_{i,j+1}$, which have the following coordinates: $P_{i,j} = (x_{ij}, y_{ij}, z_{ij})$ and $P_{i,j+1} = (x_{i,j+1}, y_{i,j+1}, z_{i,j+1})$.

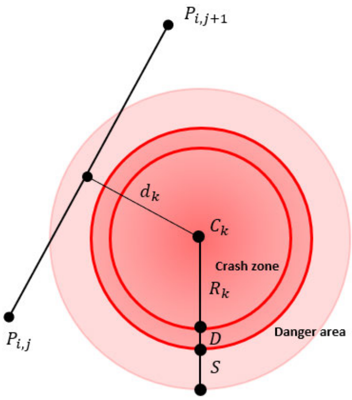

FIGURE 1. Model of a threat.

B. TERRAIN AND UAV PERFORMANCE CONSTRAINTS

Safe path planning requires complete avoidance of all obstacles in the flight path. Let K denote the set of all threats, each of which is represented by a cylinder. As shown in Fig. 1, each obstacle is defined geometrically by two main parameters: its centre coordinate C_k and its radius R_k. To accurately account for the threat cost of the UAV, the size of the UAV is considered to be D, where d_k is the distance between the UAV and the center of each threat.

The threat cost F_2, computed across waypoints $P_{i,j}$ for obstacle set K, is determined based on the schematic model of a threat illustrated above as follows:

$$\begin{cases} F_2(X_i) = \sum_{j=1}^{n-1}\sum_{k=1}^{K} T_k\left(\overrightarrow{P_{i,j}P_{i,j+1}}\right) \\ T_k\left(\overrightarrow{P_{i,j}P_{i,j+1}}\right) = \begin{cases} 0 & d_k > S+D+R_k \\ (S+D+R_k)-d_k & \\ D+R_k < d_k < S+D+R_k & \\ \infty & d_k < D+R_k \end{cases} \end{cases} \tag{2}$$

It is important to note that there are several factors that can affect the possibility of a flight device hitting an obstacle in its flight path, such as the flight path environment, positioning precision, and application. Therefore, the distance from the crash area S is referred to as the danger zone. This distance depends on the nature of the obstacles, whether static or dynamic, and the quality of the connection signal. For instance, the distance can be chosen to be several tens of meters in the case of static obstacles and several hundred meters in the case of dynamic obstacles. Additionally, the flight altitude is taken into account when calculating the global cost function, which is constrained by two given height limits - the maximum and minimum height. The height cost for the pathpoint $P_{i,j}$ is calculated as follows:

$$H_{ij} = \begin{cases} \left|h_{ij} - \dfrac{(h_{max}-h_{min})}{2}\right|, & h_{min} \le h_{ij} \le h_{max} \\ \infty, & otherwise \end{cases} \tag{3}$$

The variables h_{ij}, h_{min}, and h_{max} represent the flying height of the device relative to the ground, the minimum height, and the maximum height, respectively. To calculate H_{ij}, Equation (3) is used, which takes into account the average height and penalizes out-of-range values. By summing up all H_{ij} values for all path points, the altitude cost can be determined as follows:

$$F_3(X_i) = \sum_j^n H_{ij} \tag{4}$$

Furthermore, the evaluation of the smoothing cost involves calculating the turning angle and the climbing angle. As illustrated in Fig. 2, the turning angle ϕ_{ij} is the angle between two consecutive flight way segments: $\overrightarrow{p'_{i,j}p'_{i,j+1}}$ and $\overrightarrow{p'_{i,j+1}p'_{i,j+2}}$, projected onto the horizontal plane Oxy. Assuming k is the unit vector in the direction of the z-axis, the projected vector can be calculated as follows:

$$\overrightarrow{P'_{i,j}P'_{i,j+1}} = \vec{k} \times \left(\overrightarrow{P_{i,j}P_{i,j+1}} \times \vec{k}\right) \tag{5}$$

The turning angle is computed as follows:

$$\phi_{ij} = arctan\left(\frac{\left\|\overrightarrow{p'_{i,j}p'_{i,j+1}} \times \overrightarrow{p'_{i,j+1}p'_{i,j+2}}\right\|}{\left(\overrightarrow{p'_{i,j}p'_{i,j+1}}\right)\cdot\left(\overrightarrow{p'_{i,j+1}p'_{i,j+2}}\right)}\right) \tag{6}$$

The climbing angle, denoted as ψ_{ij}, refers to the angle between the flight way segment $\overrightarrow{P_{i,j}P_{i,j+1}}$ and its projection $\overrightarrow{p'_{i,j}p'_{i,j+1}}$ onto the horizontal plane. This value can be calculated using the following formula:

$$\psi_{ij} = arctan\left(\frac{z_{i,j+1}-z_{i,j}}{\left\|\overrightarrow{p'_{i,j}p'_{i,j+1}}\right\|}\right) \tag{7}$$

Using this information, the smoothing cost can be computed as:

$$F_4(X_i) = a_1\sum_{j=1}^{n-2}\phi_{ij} + a_2\sum_{j=1}^{n-1}\left|\psi_{ij}-\psi_{i,j-1}\right| \tag{8}$$

In this equation, a_1 and a_2 represent the penalty coefficients assigned to the turning and climbing angles, respectively.

C. GLOBAL COST FUNCTION

The global cost function which quantifies the degree of optimality in terms of safety and feasibility constraints related to the path X_i, can be defined according to equations (1) to (8) as follows:

$$F(X_i) = \sum_{k=1}^{4} b_k F_K(X_i) \tag{9}$$

where b_k $(k = 1, ..4)$ are the weight cofficients, and $F_1(X_i)$ to $F_4(X_i)$ are respectevely the costs related to the path length (Equation (1)), to the threat (Equation (2)), to the smoothness (Equation (4)) and to the flight height (Equation (8)). Here,

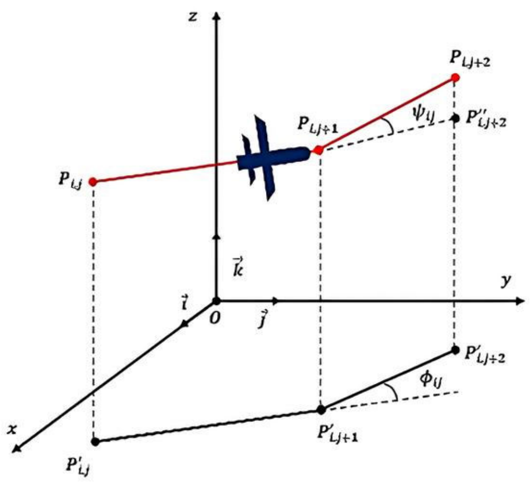

FIGURE 2. Turning and climbing angle calculation.

the decision varaible is X_i which includes n pathpoints $P_{i,j} = (x_{ij}, y_{ij}, z_{ij})$, such that $P_{i,j} \in O$, where O is the working space of UAVs.

We conclude this section by clarifying the key aspects of our model. Firstly, the 'i index' denotes the distinct waypoints in the UAV's path, essential for computing both the path length and associated threat costs. Secondly, the *'quality of the connection signal'* is fundamental for the UAV's precise positioning and swift response during navigation. Lastly, we acknowledge that modeling dynamic obstacles as larger static ones is a simplification, useful for ensuring safety but potentially restrictive under complex environments with numerous dynamic obstacles. Therefore, refining our approach to dynamic obstacle modeling will be a pivotal topic.

III. CORONAVIRUS HERD IMMUNITY OPTIMIZER

The Coronavirus Herd Immunity Optimizer (CHIO), an innovative metaheuristic optimization algorithm, was first unveiled by Al-Betar et al. in 2020 [20]. While this unique algorithm shares certain similarities with other metaheuristic algorithms, particularly in its imitation of natural phenomena, it stands apart due to its singular inspiration - the coronavirus. In mirroring the process of natural herd immunity, the algorithm incorporates elements of herd psychology, a concept lauded in the medical field as a highly effective strategy for achieving immunity against infectious diseases. The landscape of the globe has been dramatically reshaped by the Coronavirus Disease (COVID-19) pandemic, officially named by the World Health Organization (WHO) in December 2019. Originating from the bustling city of Wuhan in China, the disease was initially linked to individuals who had visited local seafood or wet markets. Early patients exhibited severe pneumonia-like symptoms and significant respiratory distress, the sources of which were initially unidentified. Despite global efforts in developing vaccines and treatment protocols, COVID-19 has propagated worldwide in distinct waves, introducing a myriad of variants [27]. This global health crisis has spurred international alliances and governments to urgently mobilize extensive resources, catalyzing the race for vaccine development [28]. However, even with multiple vaccines now available, adherence to health safety measures, such as mask-wearing, practicing social distancing, and abiding by lockdowns, remains critical in reducing the infection rate. Social distancing, promoted by the WHO as a primary strategy, seeks to curb the spread of COVID-19, a virus mainly transmitted through direct contact or exposure to contaminated objects or surfaces. The primary transmission mode is via small droplets expelled by an infected individual through sneezing, coughing, or exhalation. The effectiveness of social distancing is governed by the basic reproduction rate, signifying the number of people one infected person could potentially infect. The fatality rate, a key statistic indicating the proportion of infected individuals who succumb to the virus, is significantly influenced by individual immunity levels. Those who are elderly or suffer from chronic illnesses tend to have higher fatality rates.

Consequently, the average age of a population significantly impacts recovery rates.

A. INSPIRATION

Al-Betar and colleagues [20] conceptualized a mathematical model to achieve herd immunity against the coronavirus, resulting in the formulation of a theoretical optimization algorithm termed the Coronavirus Herd Immunity Optimizer (CHIO). This model encompasses a strategy aimed at protecting the global population from the virus by transitioning the majority of uninfected people into a resistant group incapable of further transmission. The populace within the herd immunity scenario can primarily be divided into three categories: susceptible, infected (or confirmed), and immunized (or recovered) individuals [20]. Susceptible individuals are those yet to be exposed or infected by the virus, and they stand at risk of contracting the virus through contact with infected individuals who disregard social distancing norms. Infected individuals, also termed confirmed cases, can transmit the virus to the susceptible group not observing the requisite social distancing guidelines. On the other hand, immunized individuals are protected against the virus and pose no threat to the untreated. They play a crucial role in mitigating the pandemic's spread, preventing a potential outbreak [20].

Fig. 3 outlines the population hierarchy within a herd immunity scenario, highlighting the impact of immunity acquisition on the three distinct population groups. Immunized individuals are instrumental in curbing the virus's transmission from infected to susceptible individuals, providing indirect protection to the susceptible group against the disease's spread.

B. OPTIMIZATION STEPS OF CHIO

CHIO's optimization process is outlined in six phases, as illustrated below. Algorithm 1 contains the pseudocode, and Fig. 4 displays the flowchart that depicts the workflow.

Algorithm 1 CHIO Pseudo-Code

Phase 1: **Initialization**
Initialize the parameters (HIS, BRr, $n$and $MaxAge$).
Phase 2: **Generate herd immunity population**
$x_i^j(t+1) = Lb_i + (Ub_i - Lb_i) \times rand(0,1), \forall i = 1, 2, \ldots, n$ and $j = 1, 2, \ldots .HIS$
calculate the fitness of each search agent
set $S_{vj} = 0 \forall j = 1, 2, ., HIS$
set $A_j = 0 \forall j = 1, 2, ., HIS$
Phase 3: **Herd immunity evolution**
while $(t \leq Max_{Itr})$ do
for $j = 1$ to HIS do
$isCorona\left(x^j(t+1)\right) =$ false
for $i = 1$ to n do
if $(r < \frac{1}{3} \times BRr)$ then
$x_i^j(t+1) = C\left(x_i^j(t)\right) = x_i^j(t) + r \times \left(x_i^j(t) - x_i^c(t)\right)$
$isCorona(x^j(t+1)) =$ true
else if $(r < \frac{2}{3} \times BRr)$ then
$x_i^j(t+1) = N\left(x_i^j(t)\right) = x_i^j(t) + r \times \left(x_i^j(t) - x_i^m(t)\right)$
else if $(r < BRr)$ then
$x_i^j(t+1) = R\left(x_i^j(t)\right)$
else
$x_i^j(t+1) = x_i^j(t)$
end if
end for
Phase 4: Update herd immunity population
if $f(x^j(t+1)) < f(x^j(t))$ then
$f(x^j(t)) = f(x^j(t+1))$
else
$A_j = A_j + 1$
end if
if $f\left(x^j(t+1)\right) < \frac{f(x)^j(t+1)}{\Delta f(x)} \wedge S_j = 0 \wedge is\_corona\left(x^j(t+1)\right)$ then
$S_{vj} = 1, A_j = 1$
end if
if $f\left(x^j(t+1)\right) > \frac{f(x)^j(t+1)}{\Delta f(x)} \wedge S_j = 1$ then
$S_{vj} = 2, A_j = 0$
end if
Phase 5: Check Fatality
if $\left(A_j \geq Max\_Age\right)$ *and* $\left(S_{vj} == 1\right)$ then
$x_i^j(t+1) = Lb_i + (Ub_i - Lb_i) \times rand(0,1), \forall i = 1, 2, \ldots, n$ and $j = 1, 2, \ldots .HIS$
$S_{vj} = 0$
$A_j = 0$
end if
end for
$t = t + 1$
end while

PHASE 1: INITIALIZATION

In this step, we tackle the CHIO parameters and optimization concerns. With regards to the objective function, we formulate the optimization problem as presented in Equation (10):

$$\min f(x) \quad x \in \{Lb, Ub\} \tag{10}$$

The measured objective function (or immunity rate), $f(x)$, is computed for each individual $x_i = (x_1, x_2, \ldots, x_n)$, where x_i represents the gene indexed by i, and n is the number of genes in an individual. Note that the value range for each gene is $x_i \in [Lb_i, Ub_i]$, with Lb_i representing the lowest boundary and Ub_i the highest boundary.

The CHIO algorithm utilizes four algorithmic parameters and two operational parameters. The four algorithmic parameters are (1) C_0, the number of initial infection cases triggered by an individual; (2) HIS, the population size; (3) Max_{Itr}, the total number of iterations; and (4) n, the

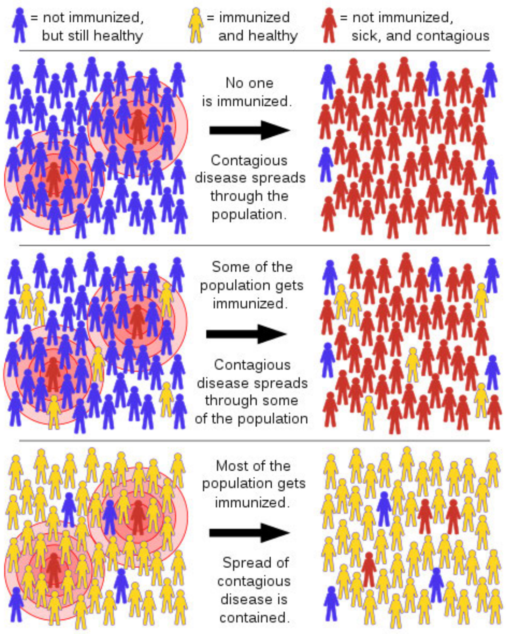

FIGURE 3. The hierarchical distribution of the population in the context of achieving herd immunity [29].

problem dimensionality. At this stage, two major control parameters of CHIO are initialized: (1) the basic reproduction rate (BRr), which regulates the operators of the algorithm by spreading the coronavirus among individuals, and (2) the maximum age of infected cases (Max_{Age}), which determines whether the infected cases recover or die.

PHASE 2: GENERATE INITIAL HERD IMMUNITY POPULATION

The CHIO generates a group of individuals that is equivalent to HIS through spontaneous or heuristic means. Within the herd immunity population (HIP), these cases are recorded in a two-dimensional matrix with a size of $HIS \times n$, arranged in the following manner:

$$HIP = \begin{bmatrix} x_1^1 & x_2^1 & \dots & x_n^1 \\ x_1^2 & x_2^2 & \dots & x_n^2 \\ . & . & \dots & . \\ . & . & \dots & . \\ x_1^{HIS-1} & x_1^{HIS-1} & \dots & x_n^{HIS-1} \\ x_1^{HIS} & x_2^{HIS} & \dots & x_n^{HIS} \end{bmatrix} \quad (11)$$

Each row j of the matrix represents a case x^j that is essentially generated, with x_i^j calculated as $x_i^j = Lb_i + (Ub_i - Lb_i) \times rand\,(0, 1)$ for every i ranging from 1 to n. The objective function, or immunity rate, is determined by utilizing Equation (10) for each situation. Additionally, the status vector (S_v) of length HIS for all cases in HIP is initialized with a value of either zero (representing a susceptible case) or one (representing an infected case). It should be noted that the number of ones in S_v is randomly initiated to be equal to C_0.

In addition to the initial representation of the status vector (S_v), where the value 0 denotes a susceptible case and 1 denotes an infected case, it is critical to explicitly state that within the scope of this phase, the 'Immune' status is designated by the number 2 in the status vector (S_v). This distinction is important for the clarity of the model's design and for maintaining the consistency with the representation used in the 'Immune case' section that follows. Therefore, we can ensure that the unique state of 'Immune' is clearly identifiable and differentiates from other states within our proposed model.

PHASE 3: EVOLVE CORONAVIRUS HERD IMMUNITY

The evolution phase represents the main enhancement loop of the CHIO. During this phase, gene x_i^j within case x^j may either remain unchanged or be modified based on the proportion of the BRr. This modification is influenced by social distancing and is governed by three distinct rules for cases that are infected, susceptible, or immune.

$$x_i^j(t+1) \leftarrow \left\{ \begin{array}{lll} x_i^j(t) & r \geq BRr & / \\ C\left(x_i^j(t)\right) & r < \frac{1}{3} \times BRr & \text{infected case} \\ N\left(x_i^j(t)\right) & r < \frac{2}{3} \times BRr & \text{susceptible case} \\ R\left(x_i^j(t)\right) & r < BRr & \text{immune case} \end{array} \right\} \quad (12)$$

Here, r is a number generator that generates values between 0 and 1. The following section describes the three rules that govern the modification of genes within cases during the evolution phase.

1) INFECTED CASE

When the value of r falls within the range of $[0, BRr/3]$, the resulting social distancing can be attributed to the modification of the gene value, denoted as $x_i^j(t+1)$. This modification is determined by calculating the difference between the current gene value and a gene value obtained from a contaminated case, denoted as x^c.

$$x_i^j(t+1) = C\left(x_i^j(t)\right) = x_i^j(t) + r \times \left(x_i^j(t) - x_i^c(t)\right) \quad (13)$$

It is important to emphasize that the selection of the value $x_i^c(t)$ is arbitrary and dependent on a status vector (S_v) associated with each contaminated case x^c. More precisely, the value i is chosen based on the condition that $c = \{i|S_v(i) = 1\}$.

2) SUSCEPTIBLE CASE

The modification of gene value $x_i^j(t+1)$ is influenced by any resulting social distancing that falls within the range of $r \in [\frac{BRr}{3}, \frac{2BRr}{3}]$. This modification is determined by the difference between the current gene value and a gene value obtained from a susceptible case x^m, where:

$$x_i^j(t+1) = N\left(x_i^j(t)\right) = x_i^j(t) + r \times \left(x_i^j(t) - x_i^m(t)\right) \quad (14)$$

It should be noted that the value $x_i^m(t)$ is randomly selected from any susceptible case x^m, taking into account the status vector (S_v) where $m = \{i|S_v(i) = 0\}$.

3) IMMUNE CASE

The value of the new gene, $x_i^j(t+1)$, is determined by the difference between the current gene and a gene extracted from an immuned case, x^v. This difference is measured within the range of $r \in [\frac{2BRr}{3}, BRr]$, representing any social disparities. The formula for calculating the new gene value is given by:

$$x_i^j(t+1) = R\left(x_i^j(t)\right) = x_i^j(t) + r \times \left(x_i^j(t) - x_i^v(t)\right) \tag{15}$$

Note that the value $x_i^v(t)$ is derived from the best immune case x^v, taking into consideration the status vector (S_v) such that $f\left(x_i^v\right) = \arg min_{j\{k|S_v(k)=2\}} f\left(x_i^j\right)$.

The distinct rules governing infected, susceptible, and immune cases, as delineated in Equation (12), are intricately designed to mirror the effects of the Basic Reproduction Rate (BRr) on gene value alterations during the evolution phase of coronavirus herd immunity. Our approach intricately intertwines the epidemiological principles with genetic modeling to reflect real-world dynamics.

1. **Infected Cases:** For a value of r less than $(BRr/3)$, the model indicates a high likelihood of virus transmission. We simulate this scenario through gene modification, which integrates genetic data from a randomly selected infected case. This represents the genetic shift occurring during actual viral transmission, showcasing how the virus proliferates among individuals.

2. **Susceptible Cases:** When r is within $(BRr/3)$ and $(2BRr/3)$, it denotes a moderate infection risk. The corresponding gene modification here involves blending genetic materials from a susceptible individual with another randomly selected susceptible case. This mirrors potential exposure and gradual genetic adaptation to the viral environment, a scenario frequently observed in populations experiencing virus outbreaks.

3. **Immune Cases:** For immune individuals, gene modifications are implemented when r is greater than $(2BRr/3)$ but less than (BRr). This reflects a substantially reduced probability of reinfection due to pre-existing immunity. The genetic alteration in this phase amalgamates genetic information from an immune individual with the strongest immune case within the population, symbolizing the bolstering of viral resistance.

In the presented section on the CHIO algorithm, the use of probabilistic thresholds derived from the Basic Reproduction Rate (BRr) is a key aspect. These thresholds are fundamental in enabling the CHIO algorithm to dynamically simulate the complexities of transmission dynamics and the evolution of immune responses within a population. The CHIO's approach to calibrating these thresholds effectively models a range of immunity levels and infection risks, providing a detailed and dynamic representation of how the virus spreads and how populations respond. This methodology underlines the probabilistic robustness of the CHIO algorithm, and it is close alignment with real-world epidemiological dynamics, as influenced by the Basic Reproduction Rate. The inclusion of these aspects in our presentation of the CHIO algorithm underscores its validity and applicability in research contexts, particularly in understanding the intricacies of coronavirus herd immunity.

PHASE 4: UPDATING HERD IMMUNITY POPULATION

The immunity rate of each case, $f(x^j(t+1))$, is calculated to determine the strength of the generated case, $x^j(t+1)$. If the immunity rate of the new case is greater than that of the actual case, $x^j(t)$, then the actual case is replaced by the new case, $x^j(t+1)$, such that $f(x^j(t+1)) < f(x^j(t))$. If $S_{vj} = 1$, the age vector, A_j, is increased by 1. The state vector (S_{vj}) is adjusted for every event, by altering the value of x^j according to the herd immune criteria, which is determined using the subsequent equation:

$$S_j \leftarrow \begin{cases} 1 & f\left(x^j(t+1)\right) < \dfrac{f(x)^j(t+1)}{\Delta f(x)} \\ & \wedge S_{vj} = 0 \wedge is\_corona\left(x^j(t+1)\right) \\ 2 & f\left(x^j(t+1)\right) > \dfrac{f(x)^j(t+1)}{\Delta f(x)} \wedge S_{vj} = 1 \end{cases} \tag{16}$$

The binary value of $is\_corona\left(x^j(t+1)\right)$ is set to 1 if case $x^j(t+1)$ inherits a new value from any infected case. Additionally, $\Delta f(x)$ represents the average significance of the immune population rates such as $\frac{\sum_{x_j}^{HIS} f(x_j)}{HIS}$. It should be noted that the levels of immunity among individuals in the population are adjusted based on the previously measured social gap. When the immunity rate of a newly produced individual surpasses the average immunity rate of the population, it indicates an increase in the population's immunity to the virus. If the newly discovered population demonstrates sufficient strength in terms of immunity to the virus, this signifies that the threshold for herd immunity has been reached.

PHASE 5: CHECK FATALITY

During this phase, if the immunity rate $f(x^j(t+1))$ of the current infected case ($Sj == 1$) cannot be improved according to the Max_Age parameter (i.e., $A_j \geq Max\_Age$), then the case is considered deceased. However, by using $x_i^j(t+1) = Lb_i + (Ub_i - Lb_i) \times rand(0,1), \forall i = 1, 2, \ldots, n$ and $j = 1, 2, \ldots .HIS$, the case is regenerated completely from scratch. A_j and S_J are both reset to 0 as well. This phase can aid in diversifying the current population and thus avoiding local optima.

PHASE 6: STOP CRITERION

The CHIO algorithm continues with phases 3 to 5 until the termination criterion is met, which is typically determined by the maximum number of iterations allowed. At this point, the population is mainly composed of susceptible and immunized cases, with the infected cases having been eliminated.

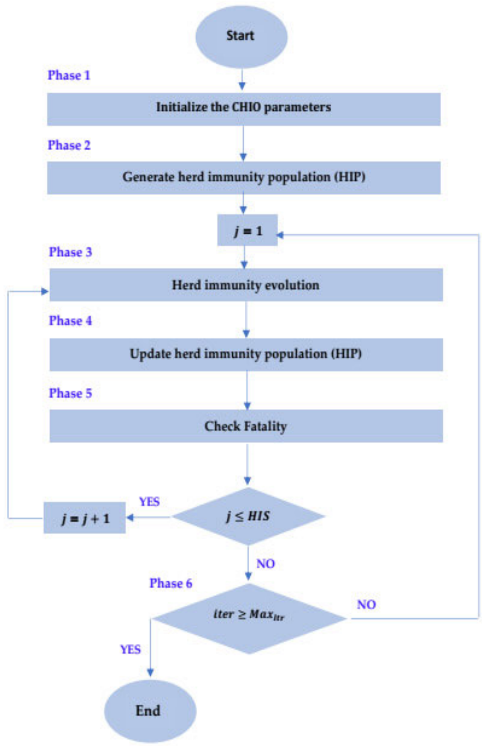

FIGURE 4. The flowchart of CHIO algorithm.

IV. THE PROPOSED PMST-CHIO

In this paper we have developed a state-of-the-art algorithm, PMST-CHIO, that is specifically designed for the safety requirements and flight constraints of UAVs in complex 3D environments. This algorithm is a modified version of the CHIO algorithm, equipped with a range of advanced features and capabilities. One of the most notable features is the introduction of a parallel multi-swarm treatment mechanism, which allows for the simultaneous and independent treatment of multiple randomly created sub-swarms. Each sub-swarm represents a herd immunity sub-population HIP associated with a specific value of the basic reproduction rate parameter. This enhances the algorithm's global exploration and exploitation capabilities and improves convergence behavior.

What sets PMST-CHIO apart is its ability to improve performance through two key mechanisms. The first mechanism involves global exploitation of the best solution found by the best CHIO laborer from the l CHIO candidates. This feature allows the algorithm to continuously learn and improve from the best solutions, ensuring that it always moves closer to the optimal outcome. The second mechanism is the ability to halt the parallel multi-swarm exploration and replace it with the best CHIO laborer's exploration when the algorithm's current iteration reaches a fixed predefined number. This ensures that the algorithm remains efficient and effective even in highly complex and dynamic environments.

In the context of UAV path planning, our CHIO optimizer's adaptation is fundamentally anchored in the global cost function, as outlined in Equation 9. This function serves as a pivotal element in evaluating the optimality of potential paths, integrating various constraints and costs associated with path length, terrain, UAV performance, threat avoidance, and smoothness. Specifically, the global cost function aggregates these individual cost elements, each quantified through respective formulae, to comprehensively assess the feasibility and safety of each path. The optimizer iteratively explores the search space, which comprises all the possible path points under the UAV's operational environment. Each path point is a potential waypoint in the UAV's journey, and the optimizer assesses these points in light of the global cost function. This approach enables a nuanced balance between direct path minimization and adherence to safety and operational constraints.

The PMST-CHIO method involves creating a global herd immunity matrix $HIP_G^{(HIS\times(n\times N_{Sub\_HIP}))}$, that consists of N_{Sub_HIP} herd immunity sub-populations. Each sub-population is represented by a unique $HIP_l^{(HIS\times n)}$, $l = \{1, \ldots, N_{Sub\_HIP}\}$ matrix and is processed by a l CHIO candidate. The elements of each matrix are generated using the same method as step 2 of a standard CHIO algorithm. The l CHIO candidate is responsible for handling its corresponding herd immunity sub-population and has its unique status variable $S_{vl}^{(1\times HIS)}$ and age vector A_l^j. All CHIO candidates begin with an equal number of initial infection cases, C_0, and a randomly generated basic reproduction rate, BRr_l,within the interval [0, 1].The herd immunity sub-populations are processed in parallel and simultaneously for a maximum number of iterations specified by Max_{P_Itr}. The best solution found by a candidate CHIO is utilized to limit the global search process to its respective CHIO owner. The top-performing CHIO then continues with the optimization process alone until the end of the iteration count, i.e., $iter = t = Max_{Itr}$. This allows for greater flexibility in computation time, with the option to either reduce or expand it.

Our PMST-CHIO algorithm, an advanced iteration of the CHIO optimizer, is designed to cater to the intricate demands of UAV path planning in complex 3D environments. This new approach hinges on a parallel multi-swarm treatment mechanism, which empowers the algorithm with enhanced global exploration capabilities. By harnessing multiple sub-swarms, each functioning independently, PMST-CHIO achieves a better search of the solution space, which is critical in UAV path planning, where navigating under a multi-dimensional environment with various constraints is paramount. The algorithm further distinguishes itself with its dual mechanisms. The first mechanism emphasizes global exploitation, leveraging the best solution identified by any CHIO laborer. This dynamic learning process ensures continual improvement, drawing the algorithm ever closer to the optimal path. The second mechanism involves a strategic pause in multi-swarm exploration, shifting the focus to the most effective CHIO laborer's trajectory when certain criteria are met. The above adaptive feature maintains the algorithm's efficiency, particularly in the rapidly changing or highly complex scenarios. Figures 5 and 6 visually encapsulate these concepts, demonstrating the PMST-CHIO's operational framework and its alignment with

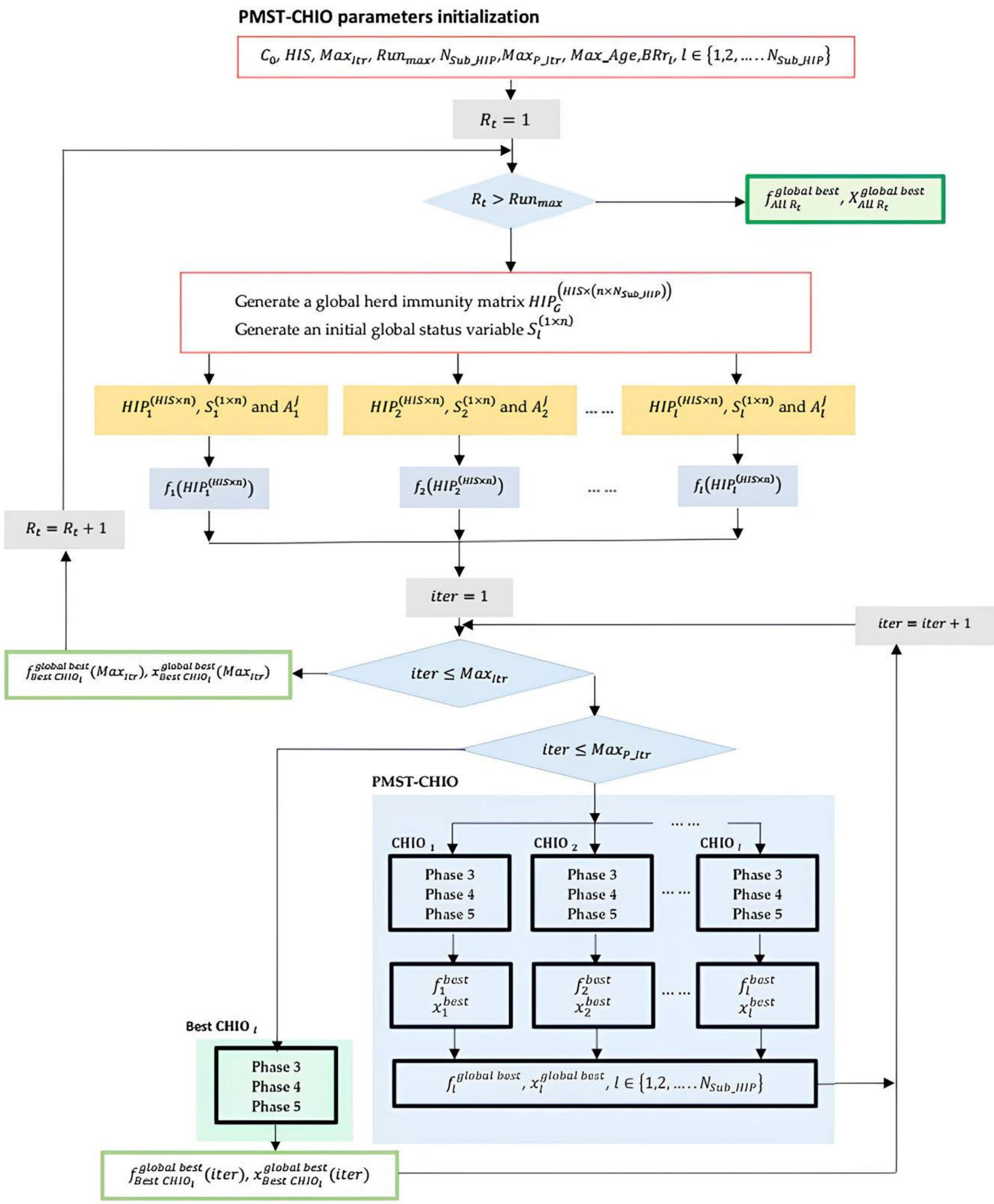

FIGURE 5. Graphical representation of PMST-CHIO.

the unique challenges of UAV navigation in the 3D landscapes.

Fig. 5 presents a detailed graphical representation of PMST-CHIO, which depicts its underlying principles and highlights the key features that set it apart from other algorithms. This figure is intended to enhance comprehension of how PMST-CHIO operates and to provide a visual overview of how it leverages a parallel multi-swarm treatment mechanism to improve exploration capabilities, as well as global exploitation and replacement mechanisms to enhance performance and convergence. Furthermore, Fig. 6 offers a comprehensive graphical representation of the relationship between PMST-CHIO and the specific challenges of operating UAVs in complex 3D environments. This figure is designed to provide an intuitive understanding of how PMST-CHIO is tailored to meet the safety requirements and flight constraints of UAVs in such environments. By examining this diagram, one can gain insight into how PMST-CHIO's advanced features, including the parallel multi-swarm treatment mechanism and global exploitation and replacement mechanisms, enable it to address the challenges posed by UAVs in complex 3D environments. Overall, Fig. 6 offers a

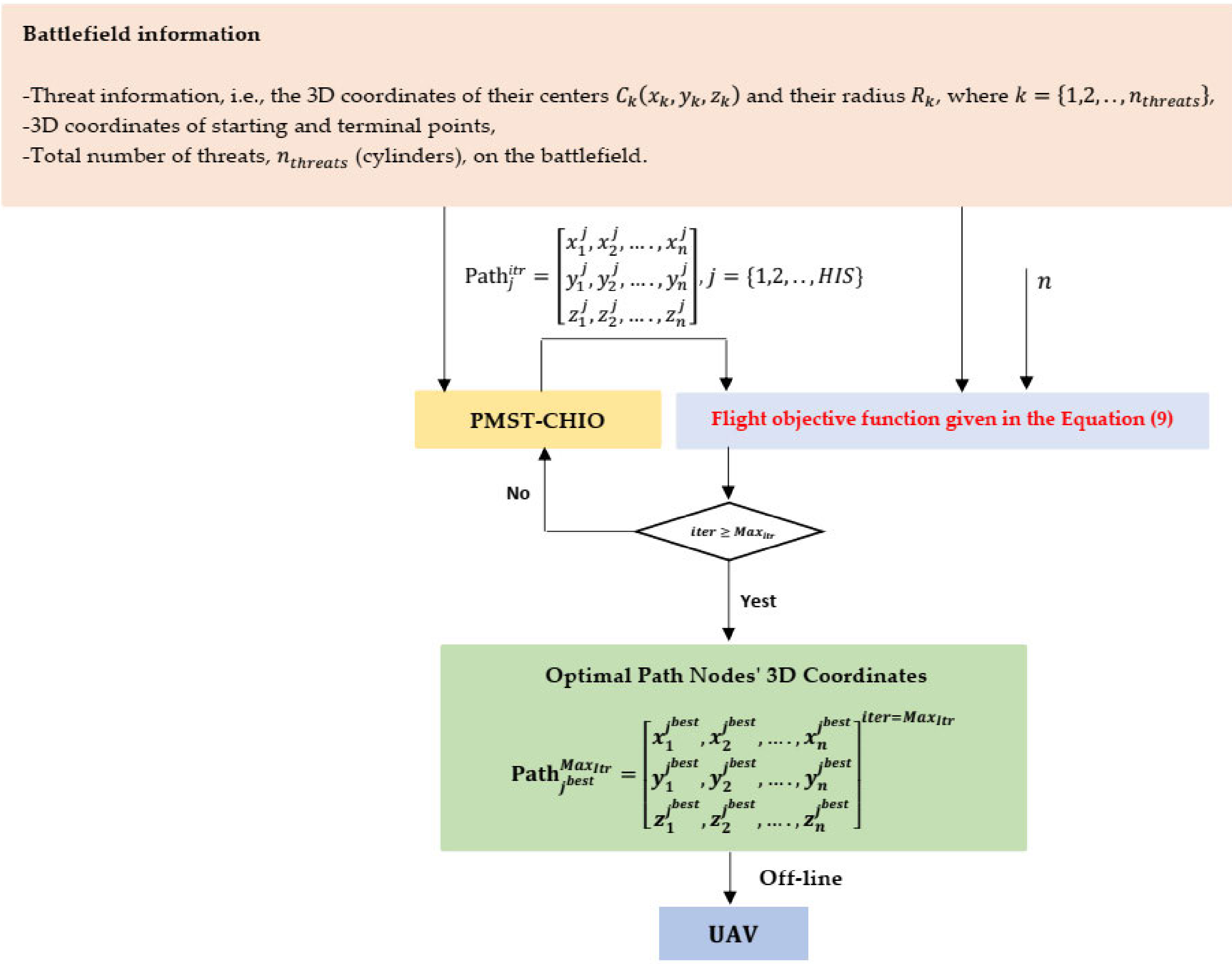

FIGURE 6. Comprehensive graphical representation of the relationship between PMST-CHIO and the specific challenges of operating UAVs in complex 3D environments.

valuable visual representation of the problem context and how PMST-CHIO is specifically designed to provide a solution for it.

V. EXPERIMENTAL SIMULATION ANALYSIS

To demonstrate the effectiveness and resilience of our proposed PMST-CHIO approach, we conducted experiments across three unique battlefields. Each battlefield posed different challenges, characterized by the presence of six, nine, and eleven threats, respectively. These threats were distributed randomly under specific conditions. We used a personal computer equipped with an Intel(R) Core (TM) i7-4510U CPU running at 2.60 GHz, supported by 6 GB of RAM and a 64-bit Windows 10 operating system. MATLAB 2022b served as our primary coding and execution platform. The battlefield scenarios were recreated using a realistic digital elevation model map, which was derived from accurate measurements taken by a lidar sensor. This map provided us with a detailed 3D terrain environment, including x, y, and z coordinates. The geographical basis for this model was a terrain structure located on Christmas Island, Australia. To ensure detailed threat representation within these simulations, each threat was modeled as a cylindrical entity. The exact center coordinates and radius of all threats are comprehensively documented in Table. 3, Table. 6, and Table. 9, corresponding to the respective battlefields. We also designated start (S) and end (T) nodes for each battlefield at specific coordinates. For battlefield 1, the coordinates were $S^1(200, 100, 150)$ and $T^1(800, 800, 150)$. For battlefield 2, they were $S^2(200, 200, 150)$ and $T^2(800, 800, 150)$. For battlefield 3, they were $S^3(200, 200, 150)$ and $T^3(780, 600, 150)$. This experimental setup allowed us to examine the performance of PMST-CHIO under various conditions, thus facilitating a comprehensive evaluation of its capabilities.

In addressing the selection of problem dimensions for our simulations, we chose dimensions of 10, 20, and 30 to represent varying levels of complexity. This approach was intended to evaluate the adaptability and effectiveness of the PMST-CHIO algorithm across different scales. We observed that increasing the problem dimensionality escalated the complexity of path optimization, influencing the algorithm performance. These findings, detailed in our analysis, demonstrate PMST-CHIO's capabilities and limitations in handling diverse operational scenarios.

In order to maintain consistency across the tests, we have established a set of control parameters for the PMST-CHIO. The parameters are as follows: the Herd Immunity (*HIS*) population size is set at 30; the number of initial infection cases, or the index case, denoted by C_0, is 1; the basic reproduction rate, BRr_l, for each *lth* CHIO candidate is randomly assigned within the range of 0 and 1, where l is any integer belonging to the set $\{1, 2, \ldots..N_{Sub\_HIP}\}$; the maximum age of infected cases, denoted as Max_{Age}, is capped at 100; the number of treated swarms or herd immunity sub-populations, denoted as N_{Sub_HIP}, is set to 20; each sub *HIP* is correlated to a single CHIO worker; the threshold iteration, represented as Max_{P_Itr}, is fixed at 9000. Furthermore, the evaluation of PMST-CHIO was performed over a maximum of 10000 iterations (denoted as Max_{Itr}, and each experiment was replicated 20 times indicated as Run_{max} to ensure reliable and statistically sound results. In order to comprehensively analyze the performance of PMST-CHIO, we calculated the best, worst, mean, and standard deviation (std.) for all results obtained. This rigorous procedure provided a broad-spectrum analysis, offering valuable insights into the operational efficiency and potential applicability of PMST-CHIO in diverse battlefield scenarios.

In the quest to understand of different algorithms in the context of simulated battlefields, the PMST-CHIO algorithm was compared to the CHIO and four distinct algorithms, under identical conditions, across three different battlefield scenarios. The considered algorithms are the Spherical Vector-based PSO (SPSO) [9], the widely recognized PSO, the Artificial Bee Colony (ABC) algorithm [30], and the Differential Evolution (DE) [31]. A comprehensive collation of the results acquired from all six algorithms, across the three simulated battlefields, is provided in Table. 4, Table. 7, and Table. 10. To delve deeper into the statistical aspects of these results, Wilcoxon's rank-sum nonparametric statistical test was employed. The results of this statistical test are available in Table. 5, Table. 8, and Table. 11, with a significance level set at 0.05. The algorithms that offered superior results and rankings are distinguished by their presentation in bold. Furthermore, the convergence behavior of the PMST-CHIO algorithm was scrutinized in direct comparison with other algorithms across all tests. The graphical depictions of convergence curves for the PMST-CHIO and its counterparts, tailored to each of the three battlefield scenarios, can be found in Fig. 7, Fig. 11, and Fig. 15. Adding another layer of visual understanding, boxplot diagrams for each battlefield have been provided in Fig. 10, Fig. 14, and Fig. 18, corresponding to battlefield 1, 2, and 3 respectively.

In these graphical representations, the black central line within each box signifies the median, while the edges of the box delineate the 25th and 75th percentiles. The whiskers stretch to incorporate the most extreme data points, excluding any outliers, which are individually plotted. Each box encapsulates results from 20 individual runs. Finally, the path planning results, as optimized by the PMST-CHIO along with the five other competing algorithms, are presented in a bird's-eye view format in Fig. 8, Fig. 12, and Fig. 16 for battlefields 1, 2, and 3 respectively. Additionally, a more immersive, 3D perspective of these results can be found in Fig. 9, Fig. 13, and Fig. 17, correspondingly.

BATTLEFIELD 1: In the initial experimental analysis corresponding to the primary battlefield, a careful examination of the data presented in Table. 2 indicates the superior performance of PMST-CHIO over its counterparts. This dominance is observed across key performance indicators, including best, worst, mean, and standard deviation metrics. Not only does PMST-CHIO consistently deliver competitive results, but it also surpasses the standard CHIO model on most comparative indices. The superior performance of PMST-CHIO can be attributed to its unique and effective mechanisms.

The innovative strategy of PMST-CHIO enables it to handle a multitude of randomly generated multi-swarms both swiftly and independently, adhering to the standard CHIO protocol. However, it differentiates itself in the application of the fundamental reproduction rate parameter, where each subset of swarms is processed utilizing a unique value of this parameter. Two pivotal mechanisms further empower PMST-CHIO. Firstly, it harnesses the best solution discovered by the leading CHIO worker to execute global exploitation. Secondly, it ceases the exploration of the parallel multi-swarms and substitutes it with the exploration undertaken by the most proficient CHIO worker. This transition is triggered when the algorithm's current iteration reaches a preset threshold. The combination of these modifications significantly boosts the global exploration and exploitation capabilities of the PMST-CHIO and improves its convergence behavior.

As illustrated in Fig. 7, the PMST-CHIO model exhibits a satisfactory convergence rate when compared with its rival algorithms. This particular strength of PMST-CHIO is further highlighted through the boxplot diagrams detailed in Fig. 10. The diagrams vividly demonstrate that PMST-CHIO holds the edge in producing the minimum average value, distinguishing itself amongst its algorithmic competitors.

Shifting the focus towards the non-parametric statistical analysis, the superior performance of PMST-CHIO is robustly supported by Wilcoxon's rank-sum test, as explicitly set forth in Table. 5. This data testifies to the algorithm's robustness, outshining all other contenders in the field. Our attention is drawn to Fig. 8 and Fig. 9, which offer an enlightening perspective on the flight paths mapped by the UAV, as calculated by PMST-CHIO, CHIO, and four alternative algorithms. The flight paths optimized by PMST-CHIO stand out for their smoothness and are notably efficient in

TABLE 3. Parameter settings for threats relative to the first battlefield.

	Threat Parameter			
Threat Number	x	y	z	R
1	400	500	100	80
2	600	200	150	70
3	500	350	150	80
4	350	200	150	70
5	700	550	150	70
6	650	750	150	80

TABLE 4. Experimental results obtained for the six experimented algorithms relative to the first battlefield.

n	Results	PMST-CHIO	CHIO	SPSO	PSO	ABC	DE
10	**Best**	**4.6811E+03**	5.3273E+03	4.9392E+03	5.0609E+03	6.3702E+03	4.7449E+03
	Worst	**4.7190E+03**	8.8052E+03	6.5273E+03	7.3500E+03	8.6630E+03	5.5602E+03
	Mean	**4.6958E+03**	6.1593E+03	5.4892E+03	6.3010E+03	7.8170E+03	5.0340E+03
	Std.	**9.8837E+00**	6.8007E+02	4.7891E+02	6.2657E+02	5.4965E+02	2.2385E+02

TABLE 5. Summarised Wilcoxon rank-sum comparisons between the PMST-CHIO algorithm as a reference and five experimented algorithms for the first battlefield.

n		PMST-CHIO vs. CHIO	PMST-CHIO vs. SPSO	PMST-CHIO vs. PSO	PMST-CHIO vs. ABC	PMST-CHIO vs. DE
10	p	6.7956E-08	6.7956e-08	6.7956e-08	6.7956e-08	6.7956e-08
	h	1	1	1	1	1
Best		1	1	1	1	1

evading threat areas, resulting in the least threat cost, further amplifying its operational efficiency. A stark contrast is observed when we examine the quality of paths produced by CHIO, PSO, and ABC, as displayed in Fig. 8 and Fig. 9. It is apparent that these algorithms struggle to deliver quality in terms of stability and the ability to circumvent local optima, leading to subpar paths. Although the remaining algorithms, specifically SPSO and DE, show potential by uncovering an acceptable optimal flight path, they are still no match for PMST-CHIO in terms of path quality. In summary, PMST-CHIO not only exhibits an impressive speed of convergence but also excels in generating optimally smooth and safe UAV flight paths.

BATTLEFIELD 2: In this experimental trial, the battlefield–which serves as the subject of our investigation–is faced with a heightened magnitude of threats, encompassing nine distinct elements distributed across the expanse of the battlefield. The challenge of path planning in this context evolves into a problem of considerable complexity, with as many as twenty dimensions to consider. The superior performance of the PMST-CHIO algorithm over its competitor algorithms is apparent across a range of performance indicators, as detailed in Table. 7. This comprehensive table demonstrates how PMST-CHIO surpasses its rivals in every category, offering the best, worst, mean, and standard deviation outcomes.

From a statistical perspective, PMST-CHIO's superiority is even more evident, outpacing all methods under consideration. Fig. 11 provides a clear visual illustration of this algorithmic edge. PMST-CHIO demonstrates not only a faster convergence to the optimal flight path but also a superior quality of the final result when compared to its competition.

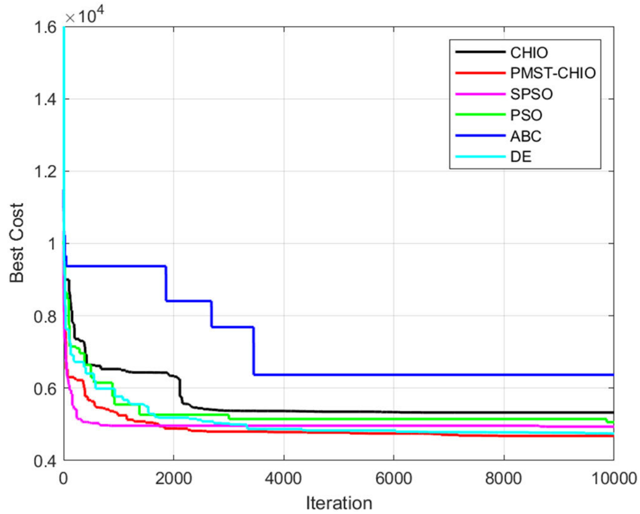

FIGURE 7. Comparative convergence curves of algorithms for battlefield 1.

Fig. 14 further amplifies this point, with the boxplot diagrams depicting the unambiguous dominance of PMST-CHIO over other algorithms in terms of performance. Moving on to Fig. 12 and Fig. 13, they offer different perspectives—overlooking and 3D views respectively—on the flight paths determined by PMST-CHIO, CHIO, and four other algorithms under consideration. The initial analysis of these

TABLE 6. Parameter settings for threats relative to the second battlefield.

Threat Number	Threat Parameter x	y	z	R
1	400	500	100	80
2	600	200	150	70
3	500	350	150	55
4	350	200	150	70
5	700	550	150	90
6	650	750	150	80
7	850	700	150	60
8	300	350	150	50
9	520	600	150	50

TABLE 7. Experimental results obtained for the six experimented algorithms relative to the second battlefield.

n	Results	PMST-CHIO	CHIO	SPSO	PSO	ABC	DE
20	Best	**4.5436E+03**	5.7364E+03	4.9864E+03	7.1948E+03	8.5860E+03	4.9243E+03
	Worst	**4.9667E+03**	6.5926E+03	6.3426E+03	9.4140E+03	1.4148E+04	7.7551E+03
	Mean	**4.7139E+03**	6.0158E+03	5.5924E+03	8.3169E+03	1.1265E+04	6.0502E+03
	Std.	**9.5968E+01**	2.7749E+02	3.4260E+02	6.1475E+02	1.4440E+03	6.8985E+02

TABLE 8. Summarised Wilcoxon rank-sum comparisons between the PMST-CHIO algorithm as a reference and *five* experimented algorithms for the second battlefield.

n		PMST-CHIO vs. CHIO	PMST-CHIO vs. SPSO	PMST-CHIO vs. PSO	PMST-CHIO vs. ABC	PMST-CHIO vs. DE
20	p	6.7956E-08	6.7956e-08	6.7956e-08	6.7956e-08	7.8980e-08
	h	1	1	1	1	1
Best		1	1	1	1	1

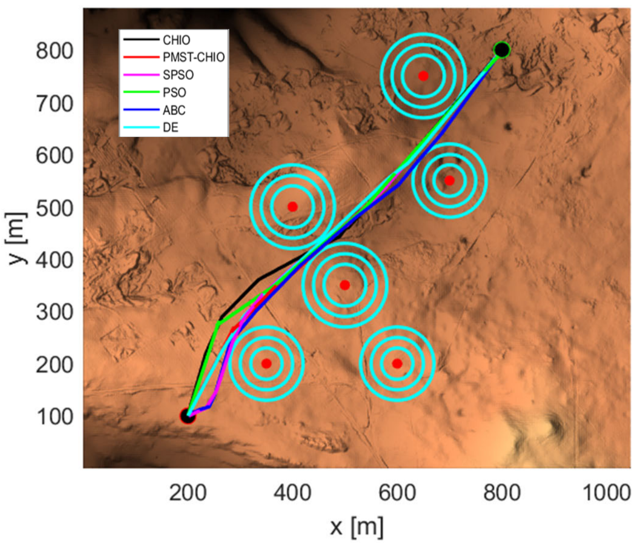

FIGURE 8. Overhead perspective of pathways created by PMST-CHIO algorithm and competing algorithms on battlefield 1.

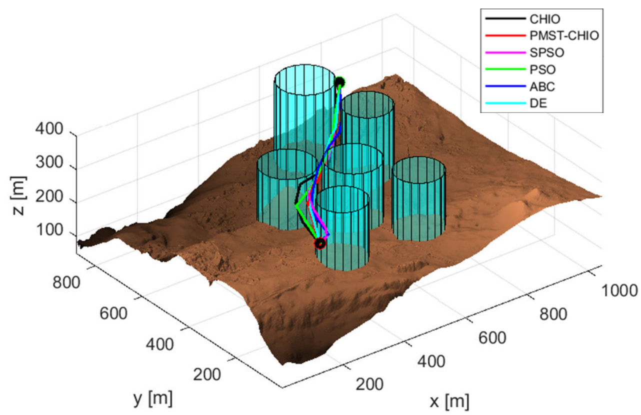

FIGURE 9. Three-Dimensional perspective of pathways produced by the PMST-CHIO algorithm and Its competitors on battlefield 1.

figures reveals that the PMST-CHIO optimized flight path stands unparalleled among all tested methods.

It shines particularly in terms of stability of the flight path and the successful circumvention of local optima. Meanwhile, the paths generated by CHIO and other algorithms under scrutiny fall short, failing to achieve the superior quality of flight paths produced by the PMST-CHIO optimization.

BATTLEFIELD 3: In the forthcoming experimental analysis centered around the intricacies of the third battleground, composed of eleven distinct threats, the proposed algorithm exhibits a notable superiority over its rivals in terms of the best, worst, mean, and standard deviation values, as distinctly evidenced in Table. 10. The PMST-CHIO, while conceding

TABLE 9. Parameter settings for threats relative to the third battlefield.

	Threat Parameter			
Threat Number	x	y	z	R
1	400	500	100	80
2	600	200	150	70
3	500	350	150	55
4	350	200	150	70
5	700	550	150	90
6	650	750	150	80
7	850	700	150	60
8	300	350	150	50
9	520	600	150	50
10	900	300	150	120
11	700	350	150	50

TABLE 10. Experimental results obtained for the six experimented algorithms relative to the third battlefield.

n	Results	PMST-CHIO	CHIO	SPSO	PSO	ABC	DE
30	**Best**	**4.9045e+03**	5.4461e+03	4.9277e+03	8.4817e+03	1.0441e+04	6.0403e+03
	Worst	**5.4021e+03**	6.6826e+03	6.9971e+03	9.3944e+03	1.8975e+04	7.3378e+03
	Mean	**5.1251e+03**	5.9104e+03	6.0165e+03	8.9221e+03	1.4903e+04	6.8063e+03
	Std.	**1.5092e+02**	3.1393e+02	6.7486e+02	2.8732e+02	2.4042e+03	3.1964e+02

TABLE 11. Summarised Wilcoxon rank-sum comparisons between the PMST-CHIO algorithm as a reference and *five* experimented algorithms for the third battlefield.

n		PMST-CHIO vs. CHIO	PMST-CHIO vs. SPSO	PMST-CHIO vs. PSO	PMST-CHIO vs. ABC	PMST-CHIO vs. DE
30	p	6.7956E-08	1.7936e-04	6.7956e-08	6.7956e-08	7.8980e-08
	h	1	1	1	1	1
Best		1	1	1	1	1

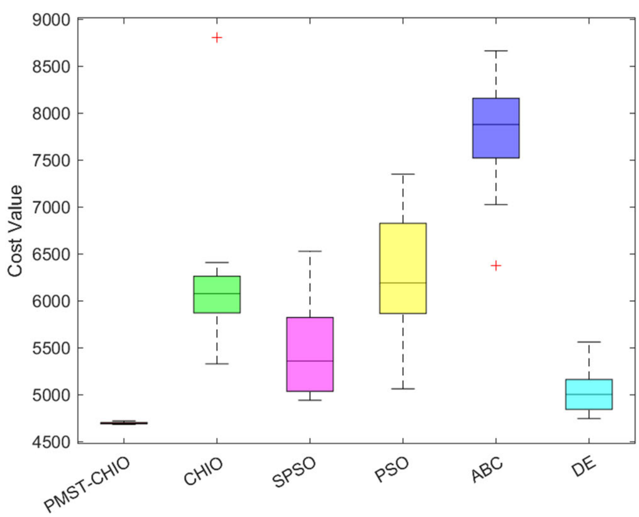

FIGURE 10. Boxplot representations comparing the performance of all algorithms on battlefield 1.

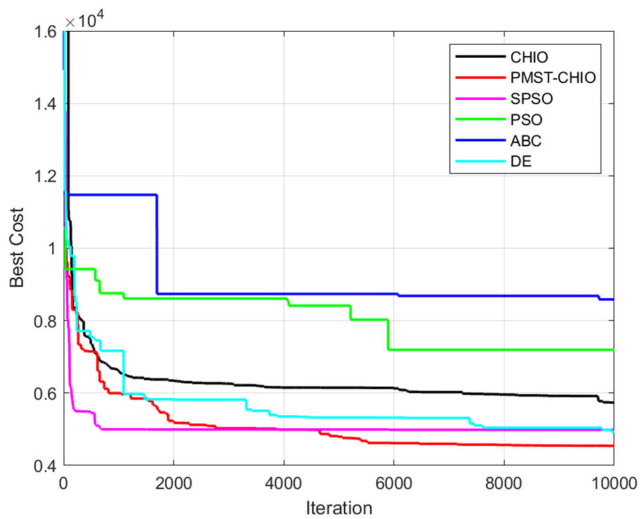

FIGURE 11. Comparative convergence curves of algorithms for battlefield 1.

a somewhat slower convergence velocity, steadily tends towards a superior fitness value, superseding all alternative algorithms (refer to Fig. 15). As corroborated by Table. 11, the PMST-CHIO emerges as the algorithm demonstrating superior performance supremacy over all other contenders. The boxed-plot visualizations encapsulated in Fig. 18 lend further credence to this superiority of PMST-CHIO, consistently outmatching its competition. Fig. 16 and Fig. 17, offering a broader perspective via overlooking and 3D views respectively, delineate the flight trajectories generated

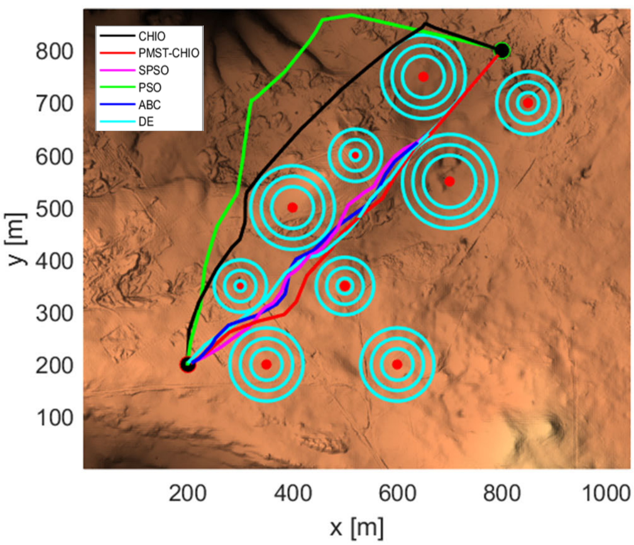

FIGURE 12. Overhead perspective of pathways created by PMST-CHIO algorithm and competing algorithms on battlefield 2.

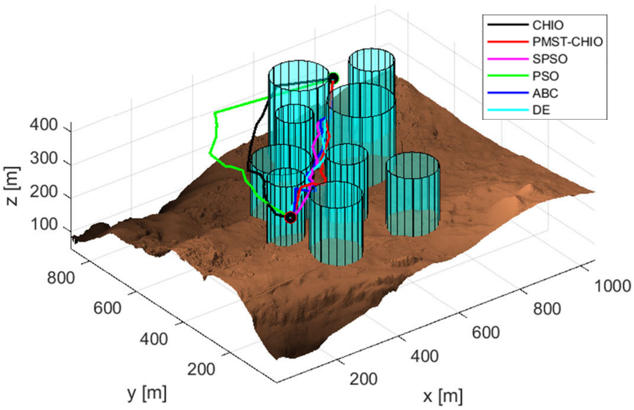

FIGURE 13. Three-Dimensional perspective of pathways produced by the PMST-CHIO algorithm and Its competitors on battlefield 2.

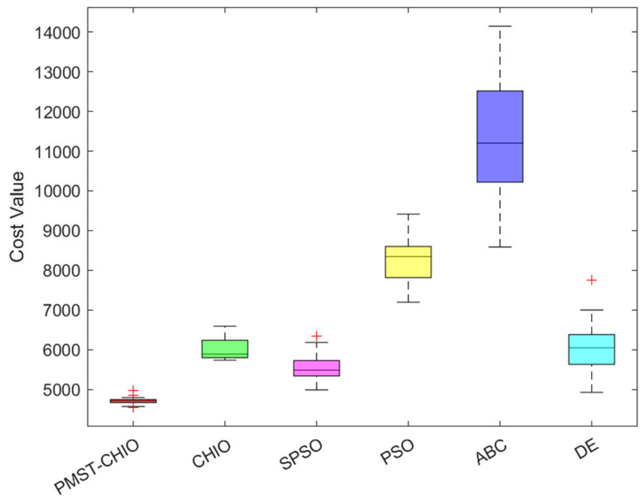

FIGURE 14. Boxplot representations comparing the performance of all algorithms on battlefield 2.

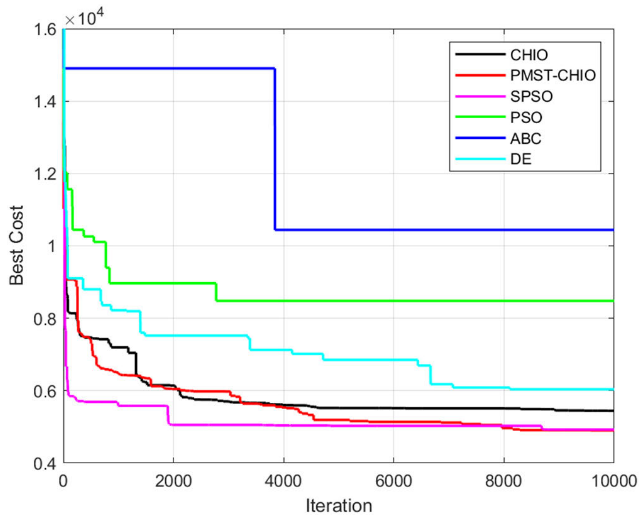

FIGURE 15. Comparative convergence curves of algorithms for battlefield 3.

by PMST-CHIO, CHIO, and four additional algorithms addressing the 30-dimension problem, given a minor adjustment to the terminal point coordinates.

Despite alterations in flight circumstances, PMST-CHIO continues to generate efficient flight paths of superior quality. Intriguingly, the optimized flight trajectories as developed by PMST-CHIO, SPSO, DE, and ABC, demonstrate a minimal level of interactions with the threat zones within the battlefield. This stands in stark contrast to the scenarios involving CHIO and PSO. These latter algorithms appear to demonstrate a marked deficiency in the effective resolution of the problem at hand, a fact clearly reflected in their respective optimized flight path configurations.

VI. ADVANTAGES, DISADVANTAGES, AND FURTHER ENHANCEMENTS OF THE PMST-CHIO ALGORITHM

Our comprehensive analysis of the PMST-CHIO algorithm, applied across three distinct battlefields, clearly demonstrates its superiority over the competing algorithms. It consistently outperforms them based on all the primary performance metrics, such as the best, worst, mean, and standard deviation values, regardless of the varying complexities and constraints of each battlefield. This distinguishing performance is attributed to its unique parallel multi-swarm treatment and dual strategies, which include leveraging the optimal solution from the lead CHIO laborer and halting parallel multi-swarm exploration upon reaching a certain threshold. The algorithm's two key strategies are:

1. Parallel Multi-Swarm Treatment: Utilizing multiple independent swarms to scan the search space, enhancing convergence speed and accuracy.

2. Dual Strategies:

- Exploiting the optimal solution from the lead CHIO laborer to guide the other swarms.

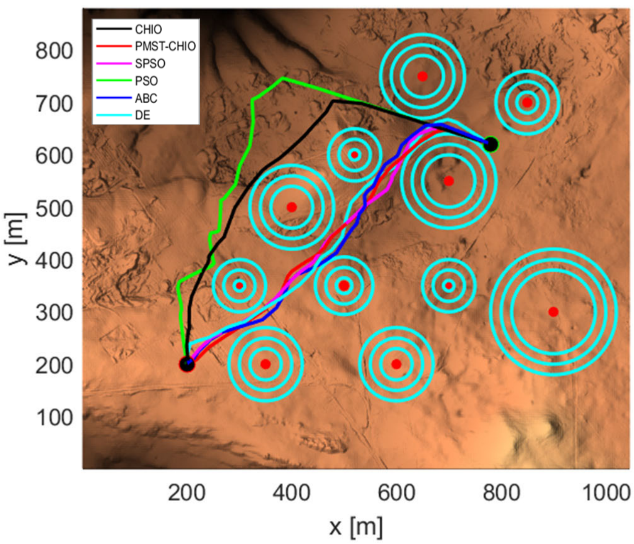

FIGURE 16. Overhead perspective of pathways created by PMST-CHIO algorithm and competing algorithms on battlefield 3.

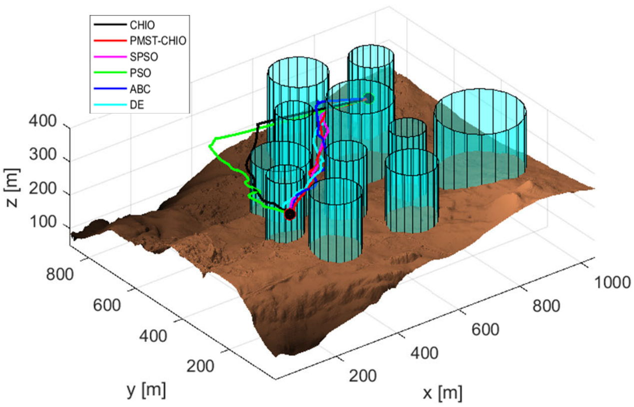

FIGURE 17. Three-Dimensional perspective of pathways produced by the PMST-CHIO algorithm and Its competitors on battlefield 3.

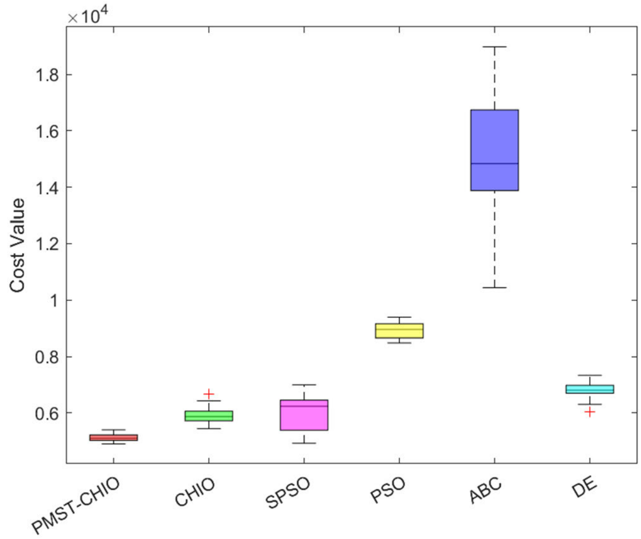

FIGURE 18. Boxplot representations comparing the performance of all algorithms on battlefield 3.

- Terminating parallel multi-swarm exploration upon reaching a user-defined satisfactory solution threshold.

The PMST-CHIO algorithm's primary advantages are:

1. Enhanced Exploration and Exploitation: Its multiple autonomous CHIO instances within sub-swarms significantly improve exploration and exploitation.

2. Optimized for Individual UAVs: Tailored for single UAV path planning, it offers improved navigational accuracy under complex 3D environments.

3. Adaptive Strategy: A strategic shift from parallel to focused exploration by the top-performing CHIO candidate, enhancing global search efficiency and convergence.

However, the PMST-CHIO algorithm has certain limitations. It shows slower convergence in complex scenarios like Battlefield 3, which has more threats. Its effectiveness heavily depends on the leading CHIO laborer's performance and the pre-set iteration threshold. To address these issues and enhance the adaptability, robustness, and efficiency, we propose the following improvements:

1. Enhancing Convergence Speed in Complex Scenarios:

- Implement adaptive parameter tuning based on scenario complexity, including a dynamic adjustment mechanism for exploration and exploitation balance.
- Integrate faster-converging algorithms, such as Genetic Algorithms and Particle Swarm Optimization to complement PMST-CHIO's strengths.
- Employ advanced machine learning techniques, e.g., deep learning models, for quicker and more accurate decision-making under varying scenarios.

2. Mitigating Dependence on the Lead CHIO Laborer:

- Develop a diversified leader selection strategy, incorporating multiple metrics for selecting leaders and reducing reliance on a single laborer.
- Promote collaborative learning and information sharing among swarms, leveraging collective intelligence to enhance overall decision-making.

3. Addressing Sensitivity to Pre-Established Thresholds:

- Introduce a dynamic threshold determination mechanism, which adapts to changing environmental conditions and algorithm performances.
- Implement feedback loops for continuous performance assessment, allowing real-time adjustment to thresholds based on the current algorithm efficacy.

4. Broader Algorithmic Improvements:

- Establish a protocol for continuous benchmarking against the newly developed and existing algorithms to ensure PMST-CHIO's competence.
- Explore and test the proposed algorithm in a wider range of applications beyond Battlefield 3, including logistics, network routing, and other complex real-world scenarios.

The algorithm's disadvantages include its complexity, increased resource intensity due to multiple autonomous

CHIO instances, and its specificity to UAV path planning. The proposed enhancements will substantially improve the algorithm performance and applicability in diverse scenarios. Future research will focus on refining convergence speed, developing a more robust algorithm via different swarm-based optimization approaches or machine learning integration, and expanding its application domains. The PMST-CHIO algorithm, with its potential to surpass the existing algorithms, marks a promising breakthrough in the swarm-based optimization.

VII. CONCLUSION

In conclusion, the PMST-CHIO algorithm has shown its effectiveness in comparison with other algorithms through a comprehensive set of experimental trials executed across three distinct battlefields. This algorithm's superior performance, evident in various measures such as best, worst, mean, and standard deviation values, coupled with its fast convergence rate and production of high-quality flight paths, underscores its superiority. The mechanisms inherent to this algorithm, including parallel multi-swarm management, global exploitation, and transitioning from parallel multi-swarm exploration to the guidance of the leading CHIO worker, have been instrumental in its success.

However, it is important to note that the PMST-CHIO algorithm is not without limitations. Its convergence speed tends to decelerate in more complex situations, and there is a significant dependence on the efficiency of the leading CHIO laborer. The algorithm is also sensitive to the pre-established threshold for parallel exploration.

Despite these challenges, the PMST-CHIO algorithm's impressive performance illustrates its value in real-world applications. Although its use has been primarily focused on UAV flight path optimization, its potential extends beyond this application, suggesting it could be an effective solution for a wide variety of optimization issues, particularly in complex environments. The algorithm's remarkable performance, even with its present constraints, demonstrates its considerable promise in numerous application areas.

REFERENCES

[1] Y.-C. Du, M.-X. Zhang, H.-F. Ling, and Y.-J. Zheng, "Evolutionary planning of multi-UAV search for missing tourists," *IEEE Access*, vol. 7, pp. 73480–73492, 2019.

[2] Q. Yang, J. Liu, and L. Li, "Path planning of UAVs under dynamic environment based on a hierarchical recursive multiagent genetic algorithm," in *Proc. IEEE Congr. Evol. Comput.*, pp. 1–8, Jul. 2020.

[3] S. Hayat, E. Yanmaz, C. Bettstetter, and T. X. Brown, "Multi-objective drone path planning for search and rescue with quality-of-service requirements," *Auto. Robots*, vol. 44, no. 7, pp. 1183–1198, Sep. 2020, doi: 10.1007/s10514-020-09926-9.

[4] V. K. Chawra and Govind. P. Gupta, "Multiple UAV path-planning for data collection in cluster-based wireless sensor network," in *Proc. 1st Int. Conf. Power, Control Comput. Technol. (ICPC2T)*, Raipur, India, Jan. 2020, pp. 194–198.

[5] Y. Liu, X. Zhang, X. Guan, and D. Delahaye, "Adaptive sensitivity decision based path planning algorithm for unmanned aerial vehicle with improved particle swarm optimization," *Aerosp. Sci. Technol.*, vol. 58, pp. 92–102, Nov. 2016.

[6] C. Qu, W. Gai, J. Zhang, and M. Zhong, "A novel hybrid grey wolf optimizer algorithm for unmanned aerial vehicle (UAV) path planning," *Knowl.-Based Syst.*, vol. 194, Apr. 2020, Art. no. 105530.

[7] H. Zhu, Y. Wang, and X. Li, "UCAV path planning for avoiding obstacles using cooperative co-evolution spider monkey optimization," *Knowl.-Based Syst.*, vol. 246, Jun. 2022, Art. no. 108713.

[8] Y. Jia, L. Qu, and X. Li, "A double-layer coding model with a rotation-based particle swarm algorithm for unmanned combat aerial vehicle path planning," *Eng. Appl. Artif. Intell.*, vol. 116, Nov. 2022, Art. no. 105410.

[9] M. D. Phung and Q. P. Ha, "Safety-enhanced UAV path planning with spherical vector-based particle swarm optimization," *Appl. Soft Comput.*, vol. 107, Aug. 2021, Art. no. 107376.

[10] Z. Han, M. Chen, S. Shao, and Q. Wu, "Improved artificial bee colony algorithm-based path planning of unmanned autonomous helicopter using multi-strategy evolutionary learning," *Aerosp. Sci. Technol.*, vol. 122, Mar. 2022, Art. no. 107374.

[11] S. Lin, F. Li, X. Li, K. Jia, and X. Zhang, "Improved artificial bee colony algorithm based on multi-strategy synthesis for UAV path planning," *IEEE Access*, vol. 10, pp. 119269–119282, 2022, doi: 10.1109/ACCESS.2022.3218685.

[12] H. Chen, Y. Liang, and X. Meng, "A UAV path planning method for building surface information acquisition utilizing opposition-based learning artificial bee colony algorithm," *Remote Sens.*, vol. 15, no. 17, p. 4312, Sep. 2023, doi: 10.3390/rs15174312.

[13] T. Erkin, N. Baktir, and S. Aslan, "A new parallel artificial bee colony algorithm for path planning of unmanned aerial vehicles," in *Proc. Innov. Intell. Syst. Appl. Conf. (ASYU)*, Oct. 2023, pp. 1–6, doi: 10.1109/ASYU58738.2023.10296613.

[14] S. Yu, Y. Li, and C. Ma, "Research on UAV trajectory planning based on artificial bee colony algorithm," in *Proc. 9th Int. Conf. Intell. Comput. Wireless Opt. Commun. (ICWOC)*, Chongqing, China, Jun. 2021, pp. 37–41, doi: 10.1109/ICWOC52624.2021.9530209.

[15] P. Kumar, S. Garg, A. Singh, S. Batra, N. Kumar, and I. You, "MVO-based 2-D path planning scheme for providing quality of service in UAV environment," *IEEE Internet Things J.*, vol. 5, no. 3, pp. 1698–1707, Jun. 2018.

[16] G. Jain, G. Yadav, D. Prakash, A. Shukla, and R. Tiwari, "MVO-based path planning scheme with coordination of UAVs in 3-D environment," *J. Comput. Sci.*, vol. 37, Oct. 2019, Art. no. 101016.

[17] A. Alihodzic, "Fireworks algorithm with new feasibility-rules in solving UAV path planning," in *Proc. 3rd Int. Conf. Soft Comput. Mach. Intell. (ISCMI)*, Nov. 2016, pp. 53–57.

[18] H. Binol, E. Bulut, K. Akkaya, and I. Guvenc, "Time optimal multi-UAV path planning for gathering its data from roadside units," in *Proc. IEEE 88th Veh. Technol. Conf. (VTC-Fall)*, Aug. 2018, pp. 1–5.

[19] F. Martínez-Álvarez, G. Asencio-Cortés, J. F. Torres, D. Gutiérrez-Avilés, L. Melgar-García, R. Pérez-Chacón, C. Rubio-Escudero, J. C. Riquelme, and A. Troncoso, "Coronavirus optimization algorithm: A bioinspired metaheuristic based on the COVID-19 propagation model," *Big Data*, vol. 8, no. 4, pp. 308–322, Aug. 2020.

[20] M. A. Al-Betar, Z. A. A. Alyasseri, M. A. Awadallah, and I. Abu Doush, "Coronavirus herd immunity optimizer (CHIO)," *Neural Comput. Appl.*, vol. 33, no. 10, pp. 5011–5042, May 2021.

[21] A. Salehan and A. Deldari, "Corona virus optimization (CVO): A novel optimization algorithm inspired from the corona virus pandemic," *J. Supercomput.*, vol. 78, no. 4, pp. 5712–5743, Mar. 2022.

[22] H. Emami, "Anti-coronavirus optimization algorithm," *Soft Comput.*, vol. 26, no. 11, pp. 4991–5023, Jun. 2022.

[23] A. M. Khalid, K. M. Hosny, and S. Mirjalili, "COVIDOA: A novel evolutionary optimization algorithm based on coronavirus disease replication lifecycle," *Neural Comput. Appl.*, vol. 34, no. 24, pp. 22465–22492, Dec. 2022.

[24] S. Safiullah, A. Rahman, S. A. Lone, S. M. S. Hussain, and T. S. Ustun, "Novel COVID-19 based optimization algorithm (C-19BOA) for performance improvement of power systems," *Sustainability*, vol. 14, no. 21, p. 14287, Nov. 2022.

[25] S. Kadkhoda Mohammadi, D. Nazarpour, and M. Beiraghi, "A novel metaheuristic algorithm inspired by COVID-19 for real-parameter optimization," *Neural Comput. Appl.*, vol. 35, no. 14, pp. 10147–10196, May 2023.

[26] Y. Yuan, Q. Shen, S. Wang, J. Ren, D. Yang, Q. Yang, J. Fan, and X. Mu, "Coronavirus mask protection algorithm: A new bio-inspired optimization algorithm and its applications," *J. Bionic Eng.*, vol. 20, no. 4, pp. 1747–1765, Jul. 2023.
[27] D. Vasireddy, R. Vanaparthy, G. Mohan, S. V. Malayala, and P. Atluri, "Review of COVID-19 variants and COVID-19 vaccine efficacy: What the clinician should know?" *J. Clin. Med. Res.*, vol. 13, no. 6, pp. 317–325, Jun. 2021.
[28] L. Soraci, F. Lattanzio, G. Soraci, M. E. Gambuzza, C. Pulvirenti, A. Cozza, A. Corsonello, F. Luciani, and G. Rezza, "COVID-19 vaccines: Current and future perspectives," *Vaccines*, vol. 10, no. 4, p. 608, Apr. 2022.
[29] Reason.com. (2020). *What's the Herd Immunity Threshold for the COVID-19 Coronavirus?*. [Online]. Available: https://reason.com/2020/05/15/whats-the-herd-immunity-threshold-for-the-covid-19-coronavirus/
[30] D. Karaboga and B. Basturk, "Artificial bee colony (ABC) optimization algorithm for solving constrained optimization problems," in *Proc. Int. Fuzzy Syst. Assoc. World Congr.*, New York, NY, USA: Springer, 2007, pp. 789–798.
[31] R. Storn and K. Price, "Differential evolution—A simple and efficient heuristic for global optimization over continuous spaces," *J. Global Optim.*, vol. 11, no. 4, pp. 341–359, 1997.

ALLOUANI FOUAD received the Engineering degree from the University of Tebessa, Algeria, in 2002, the Magister degree in engineering from the University of M'sila, Algeria, in 2006, and the Ph.D. degree in automatic control from École Nationale Polytechnique, Algeria. He is imparting his expertise and knowledge to the next generation of engineers as a Lecturer with the Department of Industrial Engineering, University of Khenchela Abbes Laghrour, Algeria. He is also a dedicated scholar in electronics and industrial control. He has a strong research inclination toward computational intelligence. His research interests include artificial neural networks, evolutionary computation, swarm intelligence, and fuzzy systems, especially their applications in process control.

ABDELAZIZ ABBOUDI received the Ph.D. degree from the University of Batna 2, Algeria. As a Prominent Member of the Scientific Research Laboratory in Materials Engineering (ISMA), he has made significant contributions to the field. From 2013 to 2019, his leadership skills shone as the Head of the Department. He is currently the Dean of the Faculty of Sciences and Technology, University of Khenchela Abbes Laghrour, Algeria. He is also a distinguished academic in materials sciences. He supervised two Ph.D. and several master's students as an active mentor. His research interests include materials engineering and automation are evident in his numerous publications, books, and instructional materials.

CHRIS HUYCK has been a Professor of artificial intelligence with Middlesex University, since 1998. His scholarly pursuits extend into the realms of computational linguistics, optimization, and several other areas within the broad field of artificial intelligence. Over the course of his tenure at Middlesex University, he has showcased his profound understanding and innovation through the publication of over 100 papers, establishing himself as a prolific and respected figure in the world of artificial intelligence research. His research interests include the intricacies of spiking neural models, which he believes offer a reasonable representation of biological neurons. Beyond this, he has dedicated considerable effort toward the development of neuropsychological models and agents constructed in neurons.

XIAO-ZHI GAO received the B.Sc. and M.Sc. degrees from Harbin Institute of Technology, China, in 1993 and 1996, respectively, and the D.Sc. (Tech.) degree from Helsinki University of Technology (now Aalto University), Finland, in 1999. Since 2018, he has been a Professor with the University of Eastern Finland, Finland. He has published more than 450 technical papers in refereed journals and international conferences. His current Google Scholar H-index is 35. His research interests include nature-inspired computing methods with their applications in optimization, data mining, machine learning, control, signal processing, and industrial electronics.

SOFIANE BOUOUDEN was born in Constantine, Algeria. He received the Ph.D. degree in control systems from the University of Constantine 1, in 2010. He is currently a Full Professor with the Department of Industrial Engineering, University of Khenchela Abbes Laghrour, Algeria. Since then, he has distinguished himself as the author of over 60 scientific publications. He has concentrated on predictive control and observation of fuzzy Takagi-Sugeno systems, control of uncertain nonlinear systems, optimization by metaheuristic algorithms (such as ant colony optimization (ACO), particle swarm optimization (PSO), and API), and robust predictive control law synthesis of uncertain multivariable systems based on linear matrix inequality (LMI) formalism. The aim of his research is to apply these principles to real-world industrial applications, focusing on sectors, such as renewable energies, motor vehicles, and biodiesel energies. These include contributions to international journals, patents, book chapters, and papers presented at international conferences. He has guided the research of numerous students, supervising seven doctoral theses, and more than 14 master's theses. His research interest includes engineering. Aside from his teaching and research responsibilities, he serves on the editorial board for various peer-reviewed journals and has been a guest editor for special issues in international journals. He has also served in key roles in the scientific community, acting as a Technical Program Committee (TPC) or International Program Committee (IPC) member or an associate editor for various international conferences. In addition, he has organized numerous scientific events, including founding the ICEECA conference.

ILYES BOULKAIBET received the B.Eng. degree in electronic engineering and the M.Eng. degree in control systems from the University of Constantine 1, Algeria, in 2004 and 2006, respectively, the first Ph.D. degree in electrical and electronic engineering from the University of Johannesburg, South Africa, in 2015, and the second Ph.D. degree in electronic engineering from the University of Constantine 1, in 2018. He is currently an Assistant Professor with the College of Engineering and Technology, American University of the Middle East, Kuwait. He is the author of more than 40 scientific publications, including international journals, book chapters, and international conferences. His research interests include machine learning applications, model predictive control systems, nonlinear control systems, natural inspired optimization theory and applications, and fault-tolerant control.

NADHIRA KHEZAMI received the Ph.D. degree in electrical engineering, automation, and industrial computing from the Central School of Lille, France, supported by a full and selective scholarship from a joint committee between Tunisia and France dedicated to higher education collaboration. She was a Visiting Professor and a Researcher with the University of Michigan, Ann Arbor, MI, USA, under the Fulbright Visiting Scholar (Teaching and Research) Program funded by the Institute of International Education and the U.S. Department of State. She is currently an Assistant Professor with the College of Engineering and Technology, American University of the Middle East, Kuwait. Her main research interests include advanced automatic control, renewable energies, embedded systems, artificial intelligence, and cyber-physical systems.

HANEN SHALL received the Diploma degree in electrical engineering and the master's (by Research) degree in electronics from the Graduate School of Engineering, University of Sfax, Tunisia, in 2009 and 2010, respectively, and the Ph.D. degree in electronics from the University of Rouen Normandy, France, in 2014. Her research activities were conducted at the Embedded Electronic Systems Research Institute (IRSEEM), Saint Etienne de Rouvray, France. She is currently an Assistant Professor with the American University of the Middle East (AUM), Kuwait. Her research interests include electronic components/systems electromagnetic compatibility (EMC), specifically the conducted immunity of electronic components: characterization and modeling, near-field measurements for EMC applications, electromagnetic simulations, and near-field radiated emission and immunity modeling of electronic equipment.